Validation of the Aura Microwave Limb Sounder middle atmosphere water vapor and nitrous oxide measurements

A. Lambert,[1] W. G. Read,[1] N. J. Livesey,[1] M. L. Santee,[1] G. L. Manney,[1,2] L. Froidevaux,[1] D. L. Wu,[1] M. J. Schwartz,[1] H. C. Pumphrey,[3] C. Jimenez,[3] G. E. Nedoluha,[4] R. E. Cofield,[1] D. T. Cuddy,[1] W. H. Daffer,[1] B. J. Drouin,[1] R. A. Fuller,[1] R. F. Jarnot,[1] B. W. Knosp,[1] H. M. Pickett,[1] V. S. Perun,[1] W. V. Snyder,[1] P. C. Stek,[1] R. P. Thurstans,[1] P. A. Wagner,[1] J. W. Waters,[1] K. W. Jucks,[5] G. C. Toon,[1] R. A. Stachnik,[1] P. F. Bernath,[6,7] C. D. Boone,[6] K. A. Walker,[6,8] J. Urban,[9] D. Murtagh,[9] J. W. Elkins,[10] and E. Atlas[11]

[1] The quality of the version 2.2 (v2.2) middle atmosphere water vapor and nitrous oxide measurements from the Microwave Limb Sounder (MLS) on the Earth Observing System (EOS) Aura satellite is assessed. The impacts of the various sources of systematic error are estimated by a comprehensive set of retrieval simulations. Comparisons with correlative data sets from ground-based, balloon and satellite platforms operating in the UV/visible, infrared and microwave regions of the spectrum are performed. Precision estimates are also validated, and recommendations are given on the data usage. The v2.2 H_2O data have been improved over v1.5 by providing higher vertical resolution in the lower stratosphere and better precision above the stratopause. The single-profile precision is $\sim$0.2–0.3 ppmv (4–9%), and the vertical resolution is $\sim$3–4 km in the stratosphere. The precision and vertical resolution become worse with increasing height above the stratopause. Over the pressure range 0.1–0.01 hPa the precision degrades from 0.4 to 1.1 ppmv (6–34%), and the vertical resolution degrades to $\sim$12–16 km. The accuracy is estimated to be 0.2–0.5 ppmv (4–11%) for the pressure range 68–0.01 hPa. The scientifically useful range of the H_2O data is from 316 to 0.002 hPa, although only the 82–0.002 hPa pressure range is validated here. Substantial improvement has been achieved in the v2.2 N_2O data over v1.5 by reducing a significant low bias in the stratosphere and eliminating unrealistically high biased mixing ratios in the polar regions. The single-profile precision is $\sim$13–25 ppbv (7–38%), the vertical resolution is $\sim$4–6 km and the accuracy is estimated to be 3–70 ppbv (9–25%) for the pressure range 100–4.6 hPa. The scientifically useful range of the N_2O data is from 100 to 1 hPa.

1. Introduction

[2] Global measurements from spaceborne instruments over the last 30 years (a) have provided important information on the middle atmosphere distributions of water vapor and nitrous oxide. In this paper we assess the quality of the daily global three-dimensional stratospheric water vapor and nitrous oxide version 2.2 data products from the Microwave Limb Sounder on the Earth Observing System Aura satellite launched in July 2004.

[3] Water vapor is a highly variable atmospheric trace gas species and the dominant greenhouse gas. It plays a major role in all fundamental atmospheric processes involving

---

[1]Jet Propulsion Laboratory, California Institute of Technology, Pasadena, California, USA.

[2]Also at Department of Physics, New Mexico Institute of Mining and Technology, Socorro, New Mexico, USA.

[3]School of GeoSciences, University of Edinburgh, Edinburgh, UK.

[4]Remote Sensing Division, Naval Research Laboratory, Washington, D. C., USA.

[5]Harvard-Smithsonian Center for Astrophysics, Cambridge, Massachusetts, USA.

[6]Department of Chemistry, University of Waterloo, Waterloo, Ontario, Canada.

[7]Now at Department of Chemistry, University of York, York, UK.

[8]Now at Department of Physics, University of Toronto, Toronto, Ontario, Canada.

[9]Department of Radio and Space Science, Chalmers University of Technology, Göteborg, Sweden.

[10]Global Monitoring Division, Earth System Research Laboratory, NOAA, Boulder, Colorado, USA.

[11]Division of Marine and Atmospheric Chemistry, University of Miami, Coral Gables, Florida, USA.

radiation, chemistry, microphysics and dynamics on a vast range of characteristic spatiotemporal scales [*Kley et al.*, 2000]. Water vapor enters the middle atmosphere from the troposphere, through the tropical transition layer (TTL), where it undergoes a ''freeze-drying'' process which renders the stratosphere extremely dry. Oxidation of methane is the dominant formation mechanism of water vapor in the stratosphere, but an increase in tropospheric methane since the 1950s can only account for about one half of the measured increase in stratospheric water vapor over this period. The photochemical stability of water vapor allows it to be used as a stratospheric tracer, however, above ∼70 km the effects of photolysis reduces the lifetime to less than 10 d.

[4] Nitrous oxide is produced almost entirely in the Earth's biosphere by natural biological activity and agricultural processes. The surface abundance of this efficient greenhouse gas has increased from ∼270 ppbv in preindustrial times to ∼319 ppbv in 2005 [*World Meteorological Organization*, 2006]. It is a well-mixed gas in the troposphere and displays a rapidly declining abundance with height in the stratosphere where it is destroyed mainly by photodissociation and also by reaction with excited oxygen forming the major source of reactive nitrogen oxides (NOx) in the stratosphere. Since the photochemical lifetime of nitrous oxide ranges from 100 a at 20 km to a few months at 40 km and is longer than dynamical timescales, it is an excellent tracer of transport processes throughout the stratosphere.

[5] NASA's Earth Observing System (EOS) Aura satellite, launched on 15 July 2004, is operated in a 98° inclination Sun-synchronous Earth orbit at an altitude of 705 km with a 1:45 P.M. ascending-node time. The Microwave Limb Sounder (MLS) [*Waters et al.*, 2006] is one of four instruments on board the Aura platform which has the main mission objective of studying ozone, air quality and climate [*Schoeberl et al.*, 2006]. MLS detects the thermal microwave emission from the Earth's limb and retrieves vertical profiles of atmospheric temperature and composition in the vertical range 8–90 km [*Livesey et al.*, 2006]. Here we present the validation of the second public release of the Aura MLS stratospheric (and mesospheric) water vapor (H₂O) and nitrous oxide (N₂O) data sets, designated version 2.2 (v2.2). The v2.2 upper troposphere and lower stratosphere H₂O retrievals for pressures >68 hPa and comparisons against measurements by hygrometers for pressures >10 hPa are discussed separately in a companion paper [*Read et al.*, 2007].

[6] The validation of the v2.2 MLS Level 2 Geophysical Product (L2GP) H₂O and N₂O retrievals, consisting of vertical profiles of the retrieved volume mixing ratios and their corresponding estimated precisions, involves assessing the data quality from the retrieval diagnostics and sensitivity studies, determining the precision and accuracy in conjunction with independent correlative measurements and providing data users with appropriate guidance on the use of the data for scientific studies. In section 2 we describe the Aura MLS measurement characteristics related to the retrieval of H₂O and N₂O, recommend a data quality control procedure, discuss the precision and resolution of the retrieved products and present the results of investigations into the instrument and forward modeling systematic errors. Comparisons with correlative measurements are presented in section 3 and the summary and conclusions are given in section 4.

2. Aura MLS Measurement Characteristics

2.1. Overview

[7] The Aura Microwave Limb Sounder [*Waters*, 1993; *Waters et al.*, 2006], an advanced successor to the MLS instrument on the Upper Atmosphere Research Satellite (UARS), is a limb sounding instrument which measures thermal emission at millimeter and submillimeter wavelengths using seven radiometers to cover five broad spectral regions. The radiometric and spectral performance of the MLS instrument is covered in detail by *Jarnot et al.* [2006] for the GHz radiometers and by *Pickett* [2006] for the THz radiometer. The standard H₂O and N₂O products are retrieved from the radiances measured by the radiometers centered near 190 GHz (R2), and 640 GHz (R4), respectively.

[8] The MLS line of sight is in the forward direction of the Aura spacecraft flight track. The Earth's limb is scanned from the surface to 90 km every 26.6 s giving 240 scans per orbit spaced at 1.5° intervals (165 km) with a total of ∼3500 vertical profiles per day and a nearly global latitude coverage from 82°S to 82°N. The viewing geometry of the MLS instrument allows the innovative use of a two-dimensional approach to the retrieval problem since the limb observations from successive scans overlap significantly which means that effects of line-of-sight gradients can be taken into account [*Livesey and Read*, 2000].

[9] At the time of writing (March 2007) reprocessing of the MLS data with the v2.2 algorithms is in progress and priority has been given initially to a set of days for which correlative measurements exist. Although fewer than 100 d covering all seasons have been used in the analysis presented here, these form a sufficient data record for a detailed investigation of the MLS data quality.

2.2. Guide to the Appropriate Use of the Data

[10] The MLS Level 2 Geophysical Product (L2GP) data consist of vertical profiles of the retrieved volume mixing ratios and their corresponding estimated precisions. The L2GP data are distributed in daily HDF-EOS version 5 swath format files [*Livesey et al.*, 2007]. The sign of the precision data field is used to flag the influence of the a priori information on the retrieved data. It is recommended that only data points with positive precision values be used, since negative precision values indicate that the a priori contributes significantly to the retrieval as discussed in section 2.5.

[11] Version 2.2 has three quality metrics available to enable screening the data to remove profiles unsuitable for scientific studies. The ''Status'' field (see Table 1) is a 32-bit integer in which the individual bits are set as necessary to indicate both instrumental and retrieval problems, e.g., instrument anomalies, potential effects of clouds, error conditions that occurred during the data processing.

[12] Any profile for which ''Status'' is an odd number should not be used in scientific studies. Nonzero but even values of ''Status'' indicate that the profile has been marked as questionable, typically because the measurements may have been affected by the presence of thick clouds. Clouds generally do not have a significant impact (outside the

Table 1. Meaning of Bits in the "Status" Field

Bit	Value[a]	Meaning
0	1	flag: do not use this profile (see bits 8–9 for details)
1	2	flag: this profile is "suspect" (see bits 4–6 for details)
2	4	unused
3	8	unused
4	16	information: this profile may have been affected by high-altitude clouds
5	32	information: this profile may have been affected by low altitude clouds
6	64	information: this profile did not use GEOS-5 temperature a priori data
7	128	unused
8	256	information: retrieval diverged or too few radiances available for retrieval
9	512	information: the task retrieving data for this profile crashed (typically a computer failure)

[a]"Status" field in L2GP file is total of appropriate entries in this column.

noise) on the stratospheric H_2O and N_2O profiles and there is no apparent need to discard data points on the basis of where "Status" values indicate the existence/influence of clouds.

[13] The "Quality" field is a floating-point number which represents how well the calculated radiances from the retrieved data were fit to the observed radiances with small values of "Quality" indicating a poor fit. We recommend only accepting profiles with "Quality" values greater than 0.9 for H_2O and 0.5 for N_2O. These thresholds typically exclude 1% of the profiles on a typical day.

[14] The "Convergence" field (introduced in the v2.2 processing) is a floating-point number which represents how close the goodness-of-fit value (χ^2) in the final retrieval step came to the predicted χ^2 based on a linear extrapolation. Generally, large values of "Convergence" indicate that satisfactory convergence was not achieved within the constraint of the maximum number of iterations allowed for the retrieval. It has not been found necessary to screen the H_2O profiles on the basis of "Convergence." There are, however, signs of poor convergence in some of the N_2O retrievals, resulting in sets of consecutive profiles that are temporally "smooth" at some levels. Data screening using the convergence field is recommended to remove these data points, therefore we recommend only accepting N_2O profiles with "Convergence" values less than 1.55. This threshold typically excludes less than 5% of the profiles on a typical day.

2.2.1. Data Artifacts
2.2.1.1. H_2O

[15] The correlative measurement comparisons in section 3 show a systematic fine-scale oscillation in the v2.2 H_2O retrievals, whereby the mixing ratio at the 31.6 hPa (26.1 hPa) level is persistently low (high) by ≤ 0.4 ppmv (8%), which is discussed further in section 2.6. Distributions of the differences in the H_2O values between these pressure levels (not shown) as a function of latitude and time indicates that larger amplitude oscillations can occur in the polar vortices
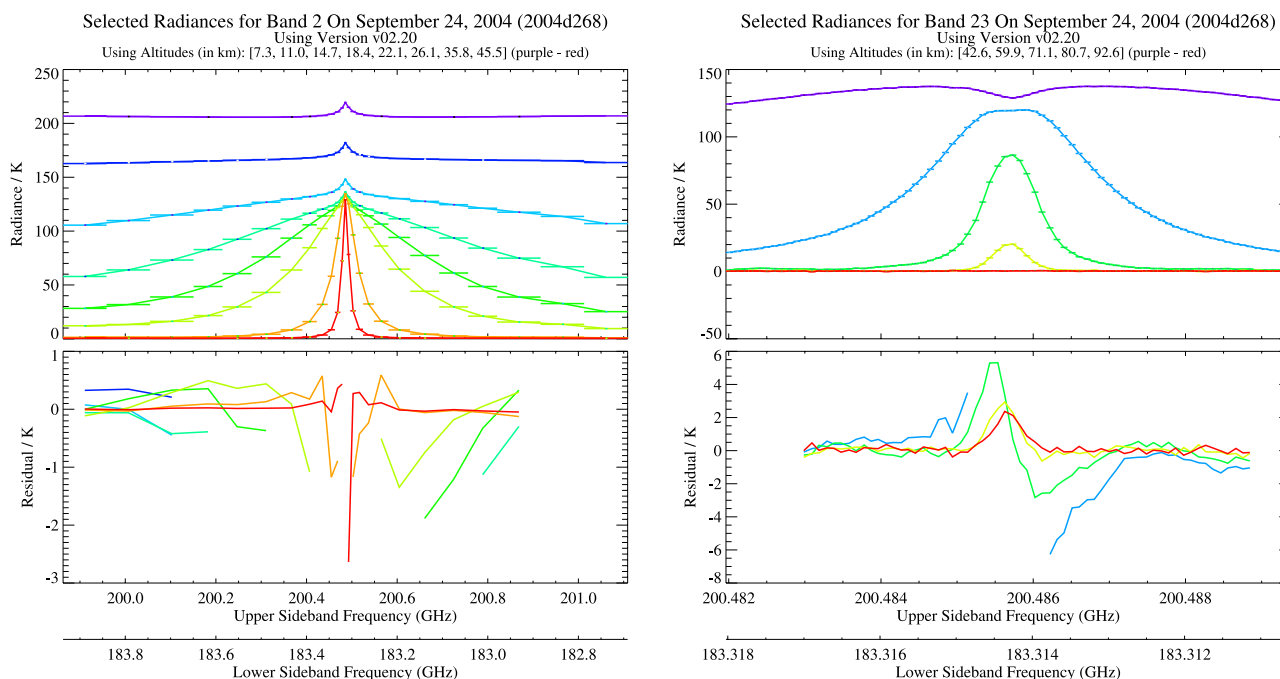

Figure 1. Sample radiance spectrum and residuals from the Aura MLS 190-GHz radiometer for (left) band 2 25-channel filterbank and (right) the band 23 129-channel digital autocorrelator spectrometer (DACS). Band 23 occupies a narrow spectral region at the center of band 2. (top) Global average radiances for a representative day (24 September 2004) for selected tangent point altitudes (purple-red). The widths of the spectral channels are denoted by horizontal bars. (bottom) Global average radiance residuals for the fit achieved by the Level 2 retrieval algorithm. Gaps along the frequency axis of the residual plots indicate channels that are not used in the retrieval. The radiance noise averaged down by the number of samples is insignificant compared to the residual spectrum.
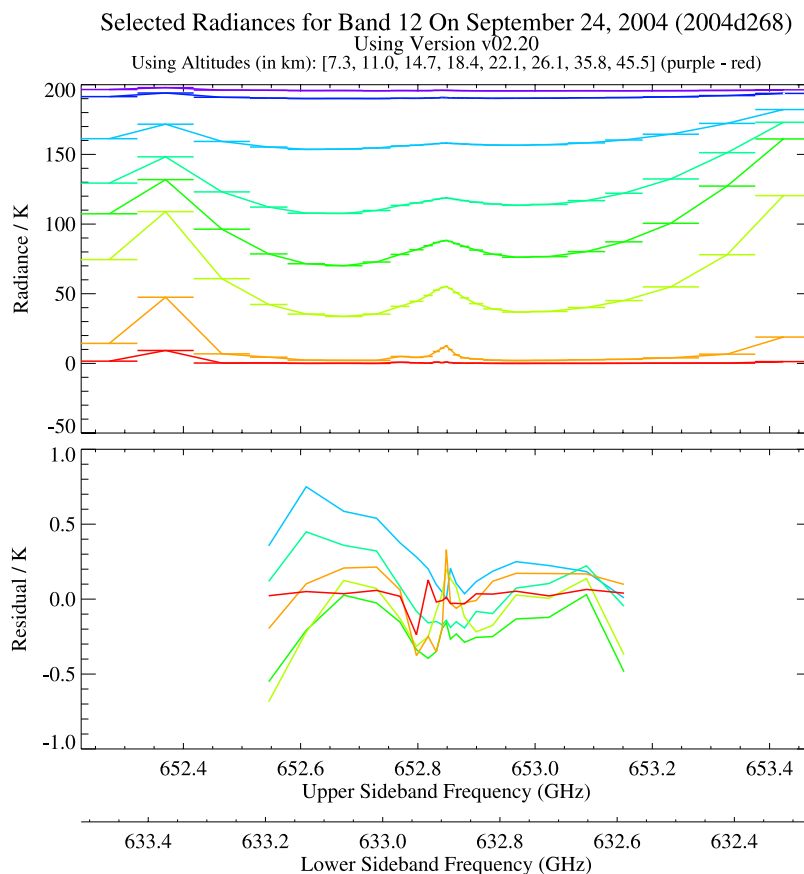
Selected Radiances for Band 12 On September 24, 2004 (2004d268)
Using Version v02.20
Using Altitudes (in km): [7.3, 11.0, 14.7, 18.4, 22.1, 26.1, 35.8, 45.5] (purple - red)

Figure 2. Sample radiance spectrum and residuals from the Aura MLS 640-GHz radiometer for band 12. Description of panels as in Figure 1.

and occasionally be reversed in sign. Rather than attempting a correction using fixed additive offsets, we suggest replacing the values at the 31.6 hPa and 26.1 hPa levels with their average for investigations that are impacted by the presence of the oscillation using the following algorithm: if $v_{31.6} < v_{38.3}$ and $v_{31.6} < v_{26.1}$ and $v_{21.5} < v_{26.1}$ then $v_{31.6} = v_{26.1} = (v_{31.6} + v_{26.1})/2$, where v_p is the volume mixing ratio at the pressure level p in hPa. This correction has not been applied to the data presented in this paper.

[16] Note that the H$_2$O retrieval uses log(mixing ratio) and the allowed H$_2$O values are constrained to be positive by applying a low bound of 0.1 ppmv.

2.2.1.2. N$_2$O

[17] The allowed N$_2$O values are restricted in the retrieval to a low bound of −40 ppbv (approximately three times the retrieval noise level in the recommended pressure range) in order to prevent a convergence problem occurring in the minimization search process. The low bound is applied at all levels, but it is only evident in the data for pressures ≤0.1 hPa, where the vertical smoothing is relaxed and the retrieval noise becomes comparable to the magnitude of the low bound value. Statistical averaging of the N$_2$O data (zonal means or longer time periods) cannot be applied successfully for pressures ≤0.1 hPa as the result will be to produce estimates with a positive bias. The N$_2$O values on the 147 hPa pressure level have a large a priori influence and practically all precisions are flagged negative at this level.

2.3. Signatures of H$_2$O and N$_2$O in the MLS Radiances

[18] Sample radiance spectra for a representative day of Aura MLS observations are shown in Figures 1 and 2 for the H$_2$O and N$_2$O retrieval, respectively. Further details concerning the MLS spectral bands and target molecules are given by *Waters et al.* [2006] and *Read et al.* [2006].

2.3.1. H$_2$O

[19] The strong H$_2$O line at 183.31 GHz dominates the spectrum in Figure 1, where Figure 1 (left) shows measurements by a 25-channel spectrometer and Figure 1 (right) shows measurements by a 129-channel digital autocorrelator spectrometer (DACS) featuring high spectral resolution in order to provide better sensitivity in the mesosphere.

[20] There is only just visible contamination from N$_2$O line emission in the channels near 201.0 GHz in the upper sideband of band 2. These channels are not included in the retrieval because they overlap with band 3 which is centered on the N$_2$O line. The residuals indicate acceptably good fits of the forward model radiances to the observed radiances of ∼2% for band 2 and of ∼5% for band 23.

2.3.2. N$_2$O

[21] In addition to the N$_2$O line at 652.83 GHz in the upper sideband, strong spectral features are present in the spectrum in Figure 2 at both sides of band 12 from ozone emission lines in the channels near 633.4 GHz (O$_3$) in the lower sideband, and near 652.3 GHz (O$_3(\nu_2)$) and 653.5 GHz (O$_3(\nu_2)$) in the upper sideband. The channels with strong contaminating lines are not included in the retrieval.

A small spectral feature is seen at the higher altitudes from contaminating species near 632.95 GHz (HNO_3 and $O_3(\nu_{1,3})$) in the lower sideband, and near 652.85 GHz ($O^{18}OO$). The residuals indicate acceptably good fits of the forward model radiances to the observed radiances of ~1% for band 12.

2.4. Retrieval Method

[22] The production of geophysical data (Level 2 data) from the calibrated observations of atmospheric limb radiances (Level 1 data) involves the Level 2 retrieval algorithms [*Livesey et al.*, 2006]. These employ an optimal estimation method [*Rodgers*, 1976, 2000] applied to the problem of a nonlinear weighted least squares minimization of a cost function involving the fit to the observed Level 1 radiance signals with regularization provided by a priori constraints. The MLS forward model [*Read et al.*, 2006; *Schwartz et al.*, 2006] takes into account the physics of the radiative transfer process and instrument specific parameters to calculate radiance estimates given a particular atmospheric state. The Level-2 processor invokes an inverse model that uses the forward model and a priori constraints in an iterative scheme, starting from an initial guess atmospheric state (obtained from a climatology), to determine the optimal atmospheric state.

[23] The MLS Level 2 processor is implemented as a series of retrieval phases [*Livesey et al.*, 2006]. In the "Core" phase the standard product retrievals of temperature/pressure (M. J. Schwartz et al., Validation of the Aura Microwave Limb Sounder temperature and geopotential height measurements, submitted to *Journal of Geophysical Research*, 2007, hereinafter referred to as Schwartz et al., submitted manuscript, 2007) and upper tropospheric humidity [*Read et al.*, 2007] are carried out and cloud detection is performed [*Wu et al.*, 2007]. This phase is then followed by the "Core+Rn" phases (n is the radiometer number) where the atmospheric species specific to the particular radiometer spectral region are retrieved. In each retrieval phase the Level 2 processor operates in parallel on ~350 data "chunks" created by subdividing the Level 1 radiance scans into contiguous measurements in a 15° span of great circle angle (typically about 10 vertical profiles); retrievals are performed for each of these chunks independently and then joined together to produce the set of retrievals for a day.

2.4.1. H_2O

[24] The standard product for H_2O in v2.2 is retrieved from the limb emission measurements at 183.31 GHz in the "Core + R2" phase from the R2 190-GHz radiometer band 2 (25-channel filter-bank spectrometer) and band 23 (129-channel digital autocorrelator spectrometer) which uses limb tangent heights with an optical depth cutoff of 0.4. Contaminating emission is present from O_3 (and excited states/isotopologues), HNO_3 and N_2O. These species are also retrieved simultaneously from other bands of the R2 radiometer, however, the N_2O retrieval from the "Core + R2" phase is currently considered a diagnostic product only and is not considered further here. The temperature and pressure data for this phase are constrained to the values retrieved from the "Core" phase (Schwartz et al., submitted manuscript, 2007). The H_2O profiles are retrieved on a pressure grid consisting of 12 levels per

decade (spacing ~1.25 km) reducing to six levels per decade for pressures <22 hPa and three levels per decade for pressures <0.1 hPa. Because of the large variation in H_2O mixing ratio, the retrieval assumes that log(mixing) ratio, and not mixing ratio itself, varies with log-pressure. The recommended pressure range for single profiles for scientific studies is 316–0.002 hPa. Further details of the retrieval for this phase relevant to the upper troposphere are presented by *Read et al.* [2007].

2.4.2. N_2O

[25] The standard product for N_2O in v2.2 is retrieved from the limb emission measurements at 652.83 GHz in the "Core + R4B" phase from the R4 640-GHz radiometer band 12 (25-channel filter-bank spectrometer). Contaminating emission is present from O_3 (and excited states/isotopologues), HNO_3, H_2O and SO_2. The SO_2 is retrieved simultaneously, but the remaining contaminant species are constrained to the values obtained from previous retrieval phases. A simultaneous temperature/pressure retrieval is also performed in this phase using the O_2 bands in the R1 (118-GHz) radiometer. The N_2O profiles are retrieved on a pressure grid consisting of six levels per decade (spacing ~2.5 km) reducing to three levels per decade for pressures <0.1 hPa. The recommended pressure range for single profiles for scientific studies is 100–1 hPa.

2.5. Precision and Resolution

[26] The formal retrieval precision estimates are the square root of the diagonal elements (variances) of the solution covariance matrix and are to be interpreted as the theoretical 1-σ uncertainties in the retrieved values. In the case of significant contribution of the a priori to the retrieved data the sign of the corresponding precision estimate is set negative by the Level 2 processor. This is effected for each pressure level where the formal precision value is greater than 50% of the a priori precision.

[27] A simple method of validating the formal retrieval precision estimates is to compare retrieved profile pairs at the intersections of ascending/descending orbits. The mean difference of the profile pairs can be useful for indicating biases in the measurement system and the observed scatter (i.e., standard deviation (SD)) about the mean differences should be ideally $\sqrt{2}$ times the precision on the individual measurements. In practice, systematic biases and increased scatter may arise from atmospheric variability (e.g., diurnal changes in concentrations, tidal effects) or residual instrument orbital effects occurring on the timescale (12 h) of the repeated measurements. The observed scatter then provides an upper limit for the precision estimates provided that the a priori has a negligible influence on the retrieval. In Figures 3 and 4 we show the results of this analysis for a large number of ascending/descending profile matches in the latitude range 50°S–50°N, where the SD values have been scaled by $1/\sqrt{2}$. Hence, in this case, the observed SD represents the statistical repeatability of the MLS measurements and the expected SD represents the theoretical 1-σ precision for a single profile.

[28] For H_2O the systematic bias in Figure 3 is small but becomes more pronounced in the mesosphere where tides may have an effect. The observed and expected SD are in reasonable agreement from 100–0.1 hPa. For pressures <0.1 hPa the observed SD is smaller than the expected
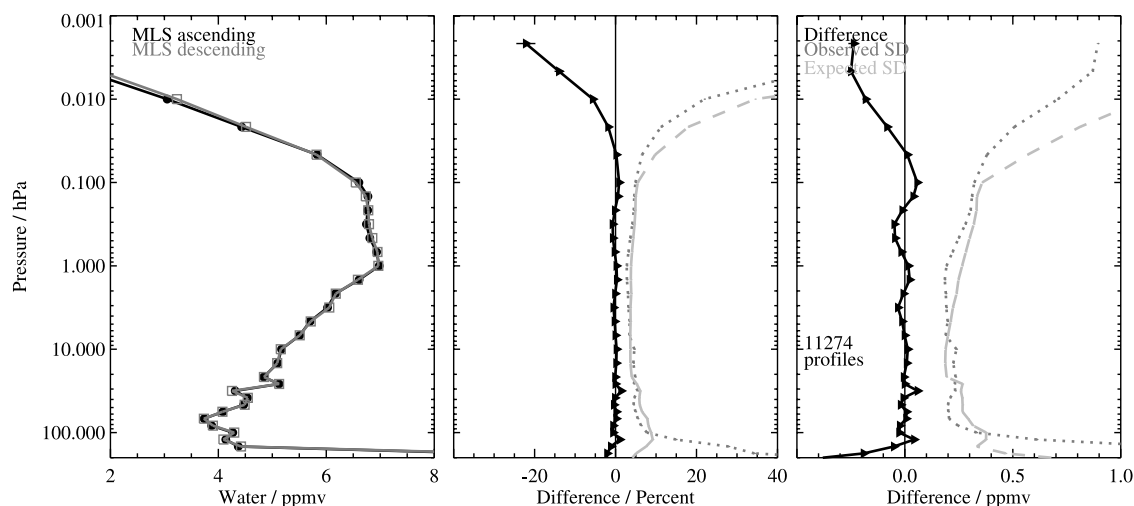
Figure 3. Comparison of MLS v2.2 H$_2$O ascending and descending orbit matching profile pairs in the latitude range 50°S–50°N averaged over 92 d. (left) Ensemble mean profiles for ascending (black circles) and descending (dark gray squares) orbit matches. (middle) Mean percentage difference profiles (black triangles) between the ascending and descending orbits; the percentage standard deviation about the mean difference (Observed SD; dark gray dotted line) and the percentage root sum square of the theoretical precisions (Expected SD; light gray dashed line) calculated by the retrieval algorithms for the two data sets. (right) As in Figure 3 (middle) except plotted in mixing ratio units. The SD values have been scaled by $1/\sqrt{2}$ and hence the observed SD represents the statistical repeatability of the measurements and the expected SD represents the theoretical 1-σ precision for a single profile.

SD indicating an increased influence of the a priori. For pressures >100 hPa atmospheric variability increases the observed SD beyond that expected from the precision estimates alone. The estimated precision on a single retrieved profile is ∼0.2–0.3 ppmv (4–9%) in the stratosphere. For N$_2$O the systematic bias in Figure 4 is small, but more pronounced at the bottom and top of the retrieval range, which is also where the observed SD is smaller then the expected SD indicating an increased influence of the a priori. The estimated precision on a single retrieved profile is ∼13–25 ppbv (7–38%) for pressures 100–4.6 hPa.

[29] The horizontal and vertical grids used in the Level 2 processing do not represent the actual spatial resolution of retrieved species as the second-order Tikhonov regularization [*Rodgers*, 2000] applied to stabilize the retrieval system degrades the intrinsic resolution [*Livesey et al.*, 2006]. The spatial resolution is obtained from examination of the averaging kernel matrices shown in Figures 5 and 6. For H$_2$O the vertical (along-track horizontal) resolution is better than 4 km (410 km) below the stratopause, but becomes worse than 10 km in the mesosphere. The across-track horizontal resolution of 7 km is set by the 190-GHz antenna pattern [*Cofield and Stek*, 2006]. For N$_2$O the vertical (along-
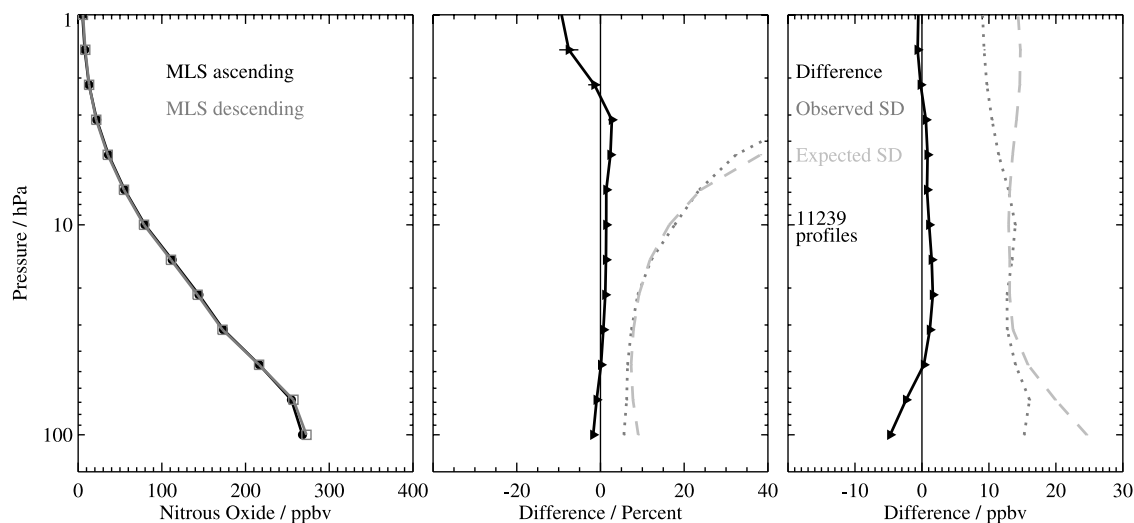
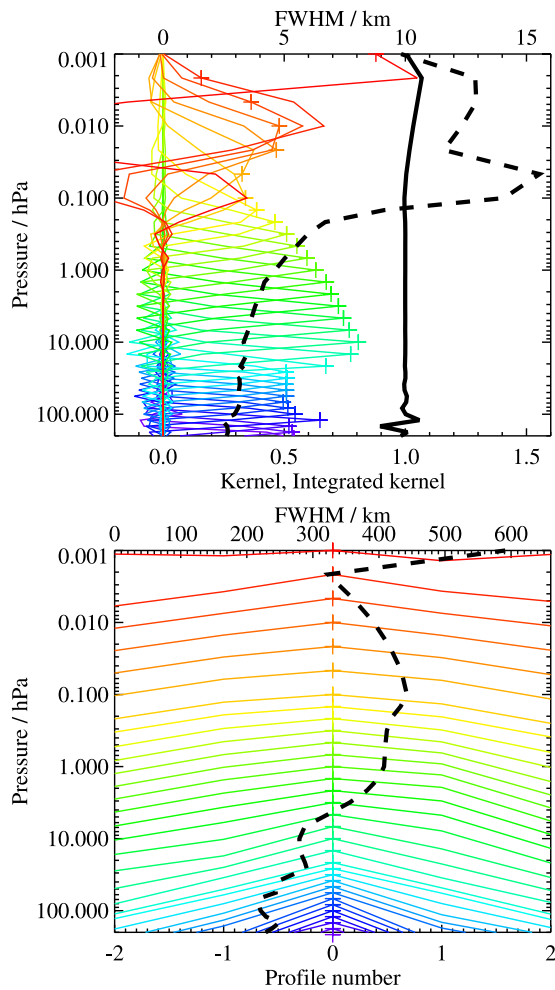**Figure 4.** As Figure 3 except for N$_2$O.

2.6. Quantification of Systematic Errors

[30] A major component of the validation of MLS data is the quantification of the various sources of systematic uncertainty. Systematic uncertainties arise from instrumental issues (e.g., radiometric calibration, field of view characterization), uncertainties in spectroscopic databases, and approximations in the retrieval formulation and implementation. This section summarizes the relevant results of a comprehensive quantification of these uncertainties that was performed for all MLS products. More information on this assessment is given by *Read et al.* [2007, Appendix A].

[31] The impact on MLS measurements of radiance (or pointing where appropriate) of each identified source of systematic uncertainty has been quantified and modeled. These modeled impacts correspond to either 2-σ estimates of uncertainties in the relevant parameters, or an estimate of their maximum reasonable errors based on instrument knowledge and/or design requirements. The effect of these perturbations on retrieved MLS products has been quantified for each source of uncertainty by one of two methods.

[32] In the first method, sets of modeled errors corresponding to the possible magnitude of each uncertainty have been applied to simulated MLS cloud-free radiances, based
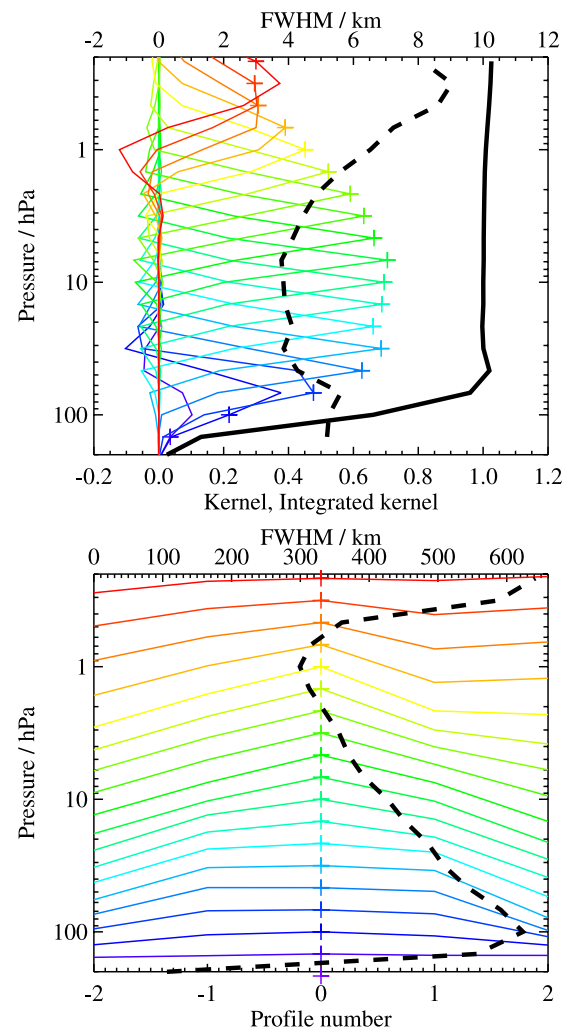

Figure 5. Typical representations of the two-dimensional (vertical and horizontal along-track) averaging kernels for the MLS H$_2$O retrieval at 35°N. The colored lines show the kernels as a function of the retrieval level. These kernels indicate the region of the atmosphere which contributes to the retrieval level denoted by the plus symbols. The solid black line shows the integrated area under each of the colored curves; values near unity indicate that almost all the information at that level was contributed by the measurement system, whereas lower values indicate increasing contributions from the a priori information. The dashed black line indicates the vertical (or horizontal) resolution as determined from the full width at half-maximum (FHWM) of the averaging kernel approximately scaled into kilometers (top axis). (top) Vertical averaging kernels (integrated in the horizontal dimension for five along-track profiles) and resolution. (bottom) Horizontal averaging kernels (integrated in the vertical dimension) and resolution. The averaging kernels are scaled such that a unit change is equivalent to one decade in pressure. Profiles are spaced at 1.5° great circle angle corresponding to 165 km along the orbit track.

track horizontal) resolution is 4–5 km (300–600 km) over most of the useful range of the retrievals and the across-track horizontal resolution of 3 km is set by the 640-GHz antenna pattern [*Cofield and Stek*, 2006].

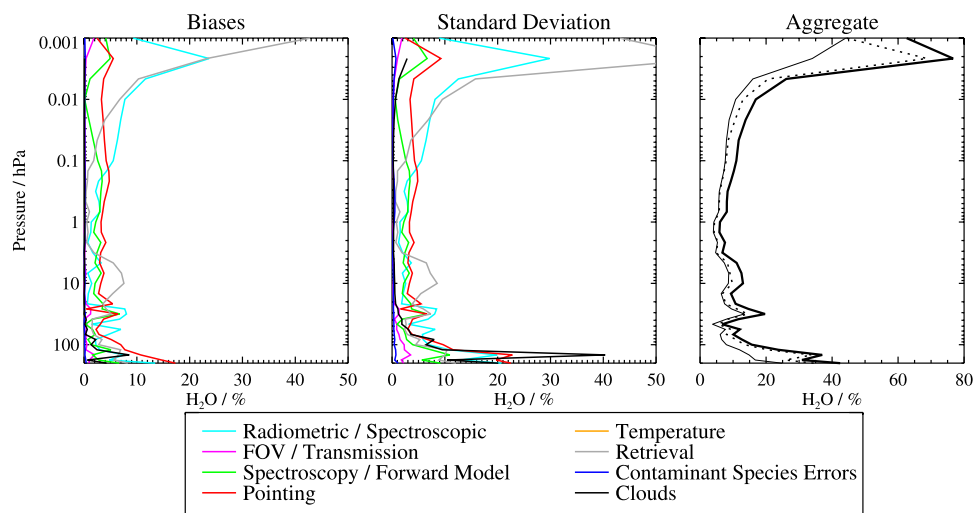**Figure 6.** As for Figure 5 but showing the MLS N$_2$O retrieval averaging kernels.

Figure 7. Estimated impact (2-σ) of various families of systematic uncertainty on the MLS H$_2$O observations with each family denoted by a different colored line. Cyan lines denote uncertainties in MLS radiometric and spectral calibration. Magenta lines show uncertainties associated with the MLS field of view and antenna transmission efficiency. Red lines depict errors associated with MLS pointing uncertainty. The impacts of uncertainties in spectroscopic databases and forward model approximations are denoted by the green line, while those associated with retrieval formulation are shown in gray. The gold lines indicate uncertainty resulting from errors in the MLS temperature product, while the blue lines show the impact of similar "knock on" errors in other species. Cloud impacts are shown as the thin black line. (left) Estimated bias. (middle) Standard deviation about the bias. (right) Root sum square of all the possible biases (thin solid line), all the additional scatter (thin dotted line), and the RSS sum of the two (thick solid line).

on a model atmosphere, for a whole day of MLS observations. These sets of perturbed radiances have then been run through the routine v2.2 MLS data processing algorithms, and the differences between these runs and the results of the "unperturbed" run have been used to quantify the systematic uncertainty in each case. The impact of the perturbations varies from product to product and among uncertainty sources. Although the term "systematic uncertainty" is often associated with consistent additive and/or multiplicative biases, many sources of "systematic" uncertainty in the MLS measurement system give rise to additional scatter in the products. For example, although an error in the ozone spectroscopy is a bias on the fundamental parameter, it has an effect on the retrievals of species with weaker signals that is dependent on the amount and morphology of atmospheric ozone. The extent to which such terms can be expected to average down is estimated to first order by these "full up studies" through their separate consideration of the bias and scatter each source of uncertainty introduces into the data. The difference between the retrieved product in the unperturbed run and the original "truth" model atmosphere is taken as a measure of the uncertainties due to retrieval formulation and numerics. Sensitivity of the retrieved mixing ratio to the a priori mean value has been assessed by performing a retrieval of the unperturbed radiances after adjusting the standard MLS a priori by a factor of 1.5.

[33] In the second method, the potential impact of some remaining (typically small) systematic uncertainties has been quantified through calculations based on simplified models of the MLS measurement system [*Read et al.*,

2007]. Unlike the "full up studies," these calculations only provide estimates of the percentage bias error introduced by the source in question; this approach is unable to quantify additional scatter for these minor sources of uncertainty.

[34] Figures 7 and 8 summarize the results of the uncertainty characterization for the MLS v2.2 H$_2$O and N$_2$O measurements, respectively. The colored lines show the magnitudes of expected biases and scatter that the various sources of uncertainty may introduce into the data, and should be interpreted as 2-σ estimates of their probable magnitude. The root sum of squares (RSS) of the aggregate error bias and aggregate error standard deviation shown in Figures 7 and 8 are considered as a proxy for the accuracy of the MLS retrievals.

[35] Although the MLS observations are unaffected by thin cirrus clouds or stratospheric aerosols, thick clouds associated with deep convection can have an impact on the MLS radiances. The MLS Level 2 data processing algorithms discard radiances identified (through comparison with predictions from a clear-sky model) as being strongly affected by clouds [*Livesey et al.*, 2006; *Wu et al.*, 2007]. The contribution of cloud effects to the systematic uncertainty, both from the presence of clouds not thick enough to be screened out by the cloud filtering and from the loss of information through omission of cloud-impacted radiances, has been quantified by adding scattering from a representative cloud field to the simulated radiances and comparing retrievals based on these radiances to the unperturbed results. The cloud-induced effects are estimated by considering only the cloudy profiles (as defined by the known amount of cloud in the "truth" field).
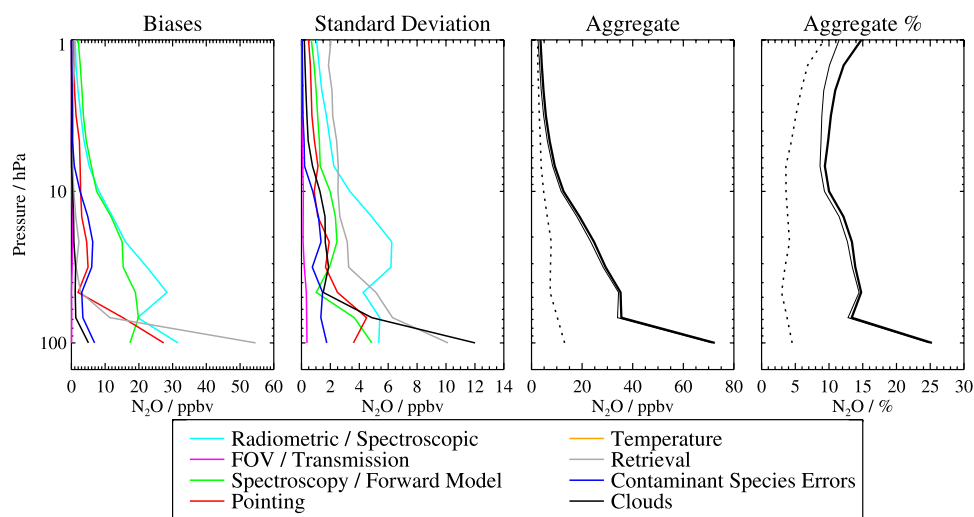
Figure 8. As for Figure 7 but showing the MLS N$_2$O error sources.

2.6.1. H$_2$O

[36] In Figure 7 the largest potential source of systematic bias for pressures >0.2 hPa is ~3% from the pointing uncertainty (red line) arising from the field of view pointing offsets between the radiometers used in the "Core" and "Core + R2" retrievals and the O$_2$ line width uncertainty. The dominant bias for pressures <0.2 hPa originates from a source contribution termed "gain compression," whereby departures from a linear response within the signal chains (cyan line: "Radiometric/Spectroscopic") introduce a spectral signature in the calibrated MLS radiances. This bias is in the range 10–25% for pressures <0.01 hPa and also has a worst case effect of ~8% in the lower stratosphere at the 31.6–26.1 hPa levels. The pointing uncertainty has a comparable effect at these levels. Compensating for gain compression in the Level 1 processing is under investigation, but has not been carried out for the v2.2 retrievals. The bias arising from the a priori (gray line: "Retrieval") is seen to be ~8% in the range 32–4.6 hPa and 10–20% in the range 0.01–0.002 hPa, but is <2% outside these regions. The uncertainty on the H$_2$O spectral line width (green line) is responsible for a bias of ~3%. Cloud-induced effects (black line) lead to negligible bias in the H$_2$O retrieval for pressures ≤68 hPa. Other potential sources of uncertainty are found to contribute negligibly to the bias. The aggregate scatter is comparable to the bias.

2.6.2. N$_2$O

[37] In Figure 8 the largest potential source of systematic bias (≤30 ppbv) over most of the profile range arises from the radiometric/spectroscopic contributions (cyan line) of gain compression, sideband fraction, and standing waves. The spectroscopic uncertainty (green line) is composed of a 20 ppbv bias in the lower stratosphere from the N$_2$O spectral line width and a worst case bias of 15 ppbv at 100 hPa from the N$_2$ continuum. The O$_3$ contaminant species uncertainty (blue line) contributes a bias of up to 6 ppbv. The pointing uncertainty (red line) is <5 ppbv for pressures ≤46 hPa rising to 27 ppbv at 100 hPa and arises from the field of view pointing offsets between the radiometers used in this retrieval (R1 and R4) and the O$_2$ line width uncertainty. The bias arising from the a priori (gray

line: "Retrieval") gives the largest contribution of 55 ppbv at 100 hPa. Cloud-induced effects (black line) lead to biases in the N$_2$O retrieval of <1 ppbv except at 100 hPa, where the bias is 5 ppbv. Other potential sources of uncertainty are found to contribute negligibly to the bias, The aggregate scatter is negligible compared to the bias.

2.7. Comparison of the v2.2 and v1.5 MLS Data Sets for H$_2$O and N$_2$O

[38] The first public release of the MLS data set was version 1.5 (v1.5) and it has been used to operationally process all data from launch to March 2007. Early validation of the v1.5 data set is discussed by *Froidevaux et al.* [2006]. Since the v1.5 H$_2$O and N$_2$O data have already been used in scientific studies [e.g., *Jimenez et al.*, 2006; *Manney et al.*, 2006], we compare these data sets and discuss their differences in this section.

2.7.1. H$_2$O

[39] In addition to the v2.2 H$_2$O product being produced on a higher vertical resolution basis grid than for v1.5, there are a number of other important changes to the retrieval. The temperature and pressure retrieval has been eliminated from the "Core + R2" phase and the optical depth cutoff for band 2 has been increased from 0.2 to 0.4. The same cutoff has been applied to band 23, which is a narrow band (10 MHz) digital autocorrelator spectrometer included the v2.2 retrieval to improve the sensitivity in the mesosphere by resolving the narrow-line Doppler-broadened emission. The spectroscopy for H$_2$O has been updated by increasing the H$_2$O line strength by 0.7% and increasing the line width by 4% (see *Read et al.* [2007] for details). Figure 9 shows the global mean v1.5 and v2.2 H$_2$O profiles, precisions and mean differences averaged over 92 d of data. The v2.2 H$_2$O data product is similar to v1.5 for pressures >0.1 hPa, except that near the stratopause v2.2 has values up to 0.5 ppmv larger and there is an oscillation present at the 31.6–26.1 hPa levels which is also seen in the comparisons to correlative data in section 3. The amplitude of oscillations at other levels reported in the v1.5 data by *Froidevaux et al.* [2006] has been reduced in v2.2. The precisions are significantly better in v2.2 especially in the mesosphere,
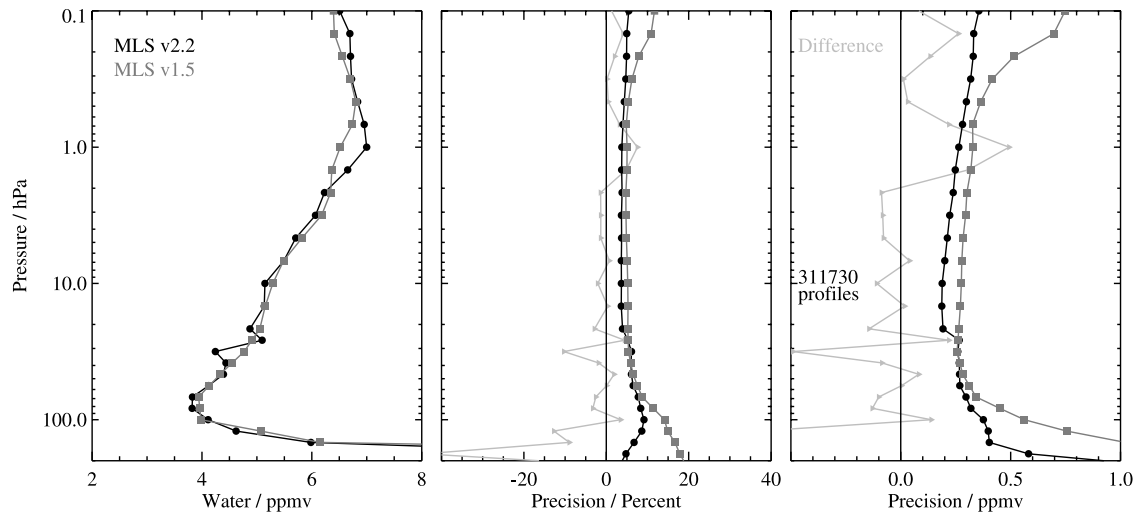
Figure 9. Comparison of MLS v2.2 H₂O with v1.5 averaged over 92 d. (left) Ensemble global mean profiles for v2.2 (black circles) and v1.5 (dark gray squares). (middle) Mean percentage difference profiles between v2.2 and v1.5 (v2.2-v1.5; light gray triangles) and the percentage theoretical precision for v2.2 (black circles) and v1.5 (dark gray squares). (right) As in Figure 9 (middle) except plotted in mixing ratio units.

where the addition of band 23 contributes to the retrieval as discussed above. For pressures <0.1 hPa the majority of the v1.5 precision data were set to negative values indicating a larger a priori influence than in v2.2.

2.7.2. N₂O

[40] The v2.2 N₂O product uses a more accurate forward model for the calculation of radiances in band 12 in the lower stratosphere (>10 hPa) than for v1.5. A linearized forward model was used for v1.5 based on precomputed radiances and derivatives for monthly climatological atmospheric states (binned in pressure and latitude). The accuracy is limited by the extent of the departure of the true state from the a priori state (linearization point) and is generally poorer in the winter polar vortexes. Figure 10 shows the global mean v1.5 and v2.2 N₂O profiles, precisions, and mean differences averaged over 92 d of data. The v2.2 N₂O product is systematically 5–15% larger than v1.5 in the region 46–2.2 hPa, but at 68 hPa and 100 hPa it is 6% and

15% smaller, respectively. The v2.2 N₂O product has slightly better precision values than in v1.5.

[41] In the lower stratosphere (≥68 hPa) polar vortex and near vortex regions the v1.5 linear forward model approximation for the N₂O retrieval occasionally led to unrealistically high biases which can be seen in Figure 11. An offline postprocessing data mask was made available for the v1.5 N₂O data [*Livesey et al.*, 2005] to screen out the biased data points (not applied in Figure 11 shown here). However, as the comparison in Figure 11 shows, these high biases have been eliminated in the v2.2 data through the use of a more accurate forward model.

3. Correlative Data Comparisons

[42] We assess the accuracy of the Aura MLS v2.2 H₂O and N₂O measurements using correlative data from spaceborne, ground-based and balloon platforms. All the com-
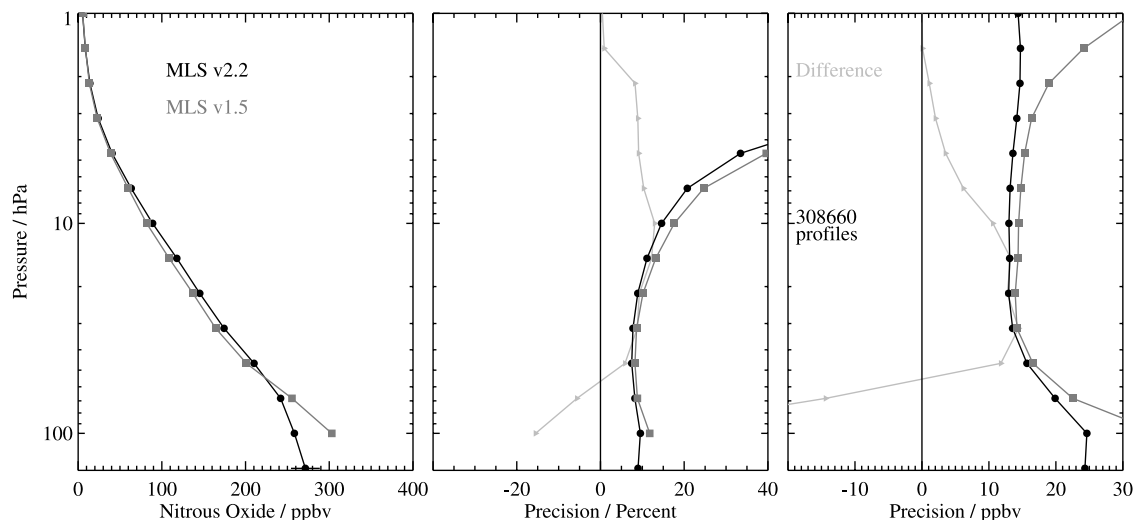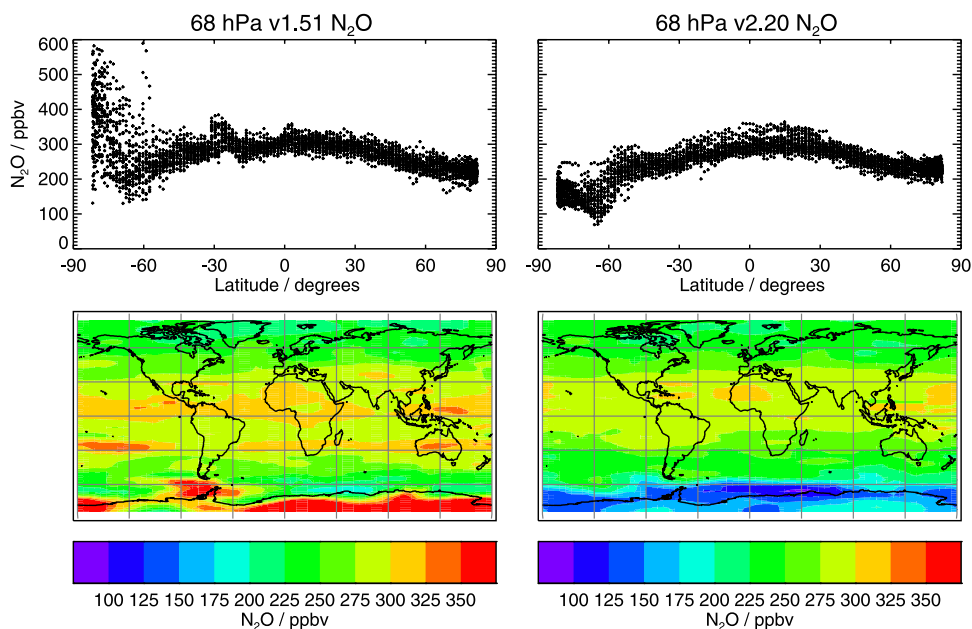

Figure 10. As Figure 9 except for N₂O.

Figure 11. Comparison of (left) MLS v1.5 to (right) MLS v2.2 N$_2$O on 17 September 2005 for the 68 hPa pressure surface. (top) Scatterplots of the N$_2$O mixing ratio as a function of latitude. (bottom) Gridded maps of the distribution of the N$_2$O mixing ratio. Anomalously high values of N$_2$O in the Southern Hemisphere polar vortex retrieved in the v1.5 processing have been eliminated in v2.2.

parisons have been performed using simple temporal and geometric spatial coincidence matching of the MLS profiles with the correlative instrument. In order to calculate differences, the correlative profiles were first linearly interpolated in log-pressure to the fixed MLS retrieval pressure grid used for a particular species. Individual profile comparisons for the balloon data are presented on their native pressure surfaces. Since in most cases the vertical resolution of the correlative measurements is comparable to that of MLS, no further processing involving averaging kernel smoothing has been applied, except as described in section 3.2 for the ground-based data. For the spaceborne and ground-based data the statistics presented are (1) the ensemble global mean species profiles of the collocated matches for both instruments, (2) the mean percentage and absolute species differences between the two instruments (MLS – "correlative"), (3) the observed standard deviations (SD) about the mean differences, and (4) the expected standard deviations calculated from the root sum square of the precisions on the species measurements from the two instruments.

3.1. Spaceborne Instruments

[43] In this section we present contemporaneous measurement comparisons from a variety of solar occultation and limb-emission instruments operating in the UV/visible, infrared and microwave wavelength regions. The latitude and time sampling of the comparisons with each of the correlative instruments is shown in Figure 12.

3.1.1. ACE-FTS

[44] The Atmospheric Chemistry Experiment Fourier Transform Spectrometer (ACE-FTS) [*Bernath et al.*, 2005] was launched in August 2003 on the Canadian Space Agency SCISAT-1 satellite into a 74° inclination orbit and uses high-resolution (0.02 cm^{-1}) infrared solar occultation in the spectral region 2.3–13.3 μm (750–4400 cm^{-1}) to measure

atmospheric temperature and concentrations of more than 20 species, including H$_2$O and N$_2$O which are retrieved using selected microwindows in the 953–2000 cm^{-1} and 1121–2668 cm^{-1} range, respectively. Nominally, fifteen sunrise and sunset profiles are obtained per day. The latitude coverage is 85°S–85°N and the vertical range is from 5 km (or cloud top) to 150 km with a typical vertical resolution of 4 km with typical precisions of <5% for H$_2$O and <5% for N$_2$O. The version 2.2 ACE-FTS data are used here [*Boone et al.*, 2005].

[45] Analyses in equivalent latitude/potential temperature coordinates comparing both H$_2$O and N$_2$O observed by ACE-FTS and MLS during several multiday intervals (using v2.2 MLS data), and comparing the evolution over the entire 2004/2005 Arctic winter (using v1.5 MLS data), are shown in a companion paper by *Manney et al.* [2007]. These analyses show good overall agreement in the morphology and timing of observed features in the two data sets.

[46] Figures 13 and 14 and compare all coincident profiles obtained within ±1° in latitude, ±8° in longitude, and ±12 h from 121 d of ACE-FTS data.

3.1.1.1. H$_2$O

[47] Figure 13 shows very good agreement to better than ±5% for nearly the entire pressure range 68–0.004 hPa (apart from the 31.6–26.1 hPa levels). The observed and expected SD are in good agreement, with the observed SD becoming smaller than the expected SD for pressures <0.1 hPa in the mesosphere; indicating an increasing a priori influence on the MLS data since the precisions on the ACE-FTS data (not shown) do not change markedly. Very similar results were found when the analysis was repeated for the separate ACE-FTS sunrise/sunset events (not shown).
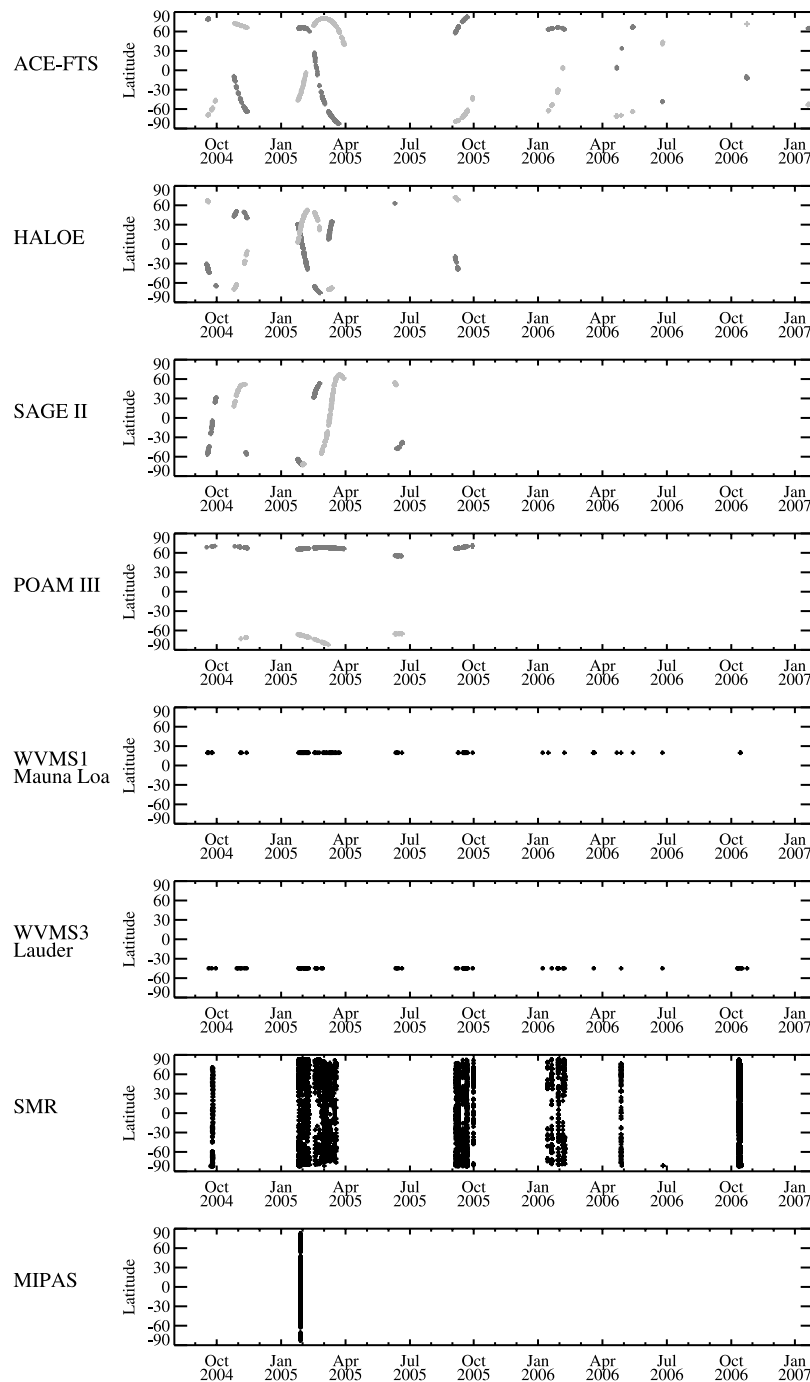
Figure 12. Sampling distributions in latitude and time of the collocated coincident matches of the v2.2 MLS data with the spaceborne and ground-based correlative instruments. For the solar occultation instruments the sunrise and sunset events are denoted by the dark gray and light gray symbols, respectively.

3.1.1.2. N₂O

[48] Figure 14 shows very good agreement with ACE-FTS to better than ±5% for nearly the entire pressure range 100–1 hPa with a low bias (up to −5%) in MLS for pressures >32 hPa and a high bias (up to +5%) at lower pressures. The latitudinal distribution of the mean differences is presented in Figure 15, where it is seen that MLS v2.2 N₂O is systematically lower at nearly all latitudes in the pressure range 100–32 hPa. This also shows the

separate ACE-FTS sunrise/sunset events and in general the sunrise events show smaller biases (MLS–ACE-FTS) for the pressure levels 46–10 hPa than do the sunset events. The observed SD is smaller than the expected SD for pressures <6.8 hPa.

3.1.2. HALOE

[49] The Halogen Occultation Experiment (HALOE) [*Russell et al.*, 1993] was launched on the Upper Atmosphere Research Satellite (UARS) into a 57° inclination
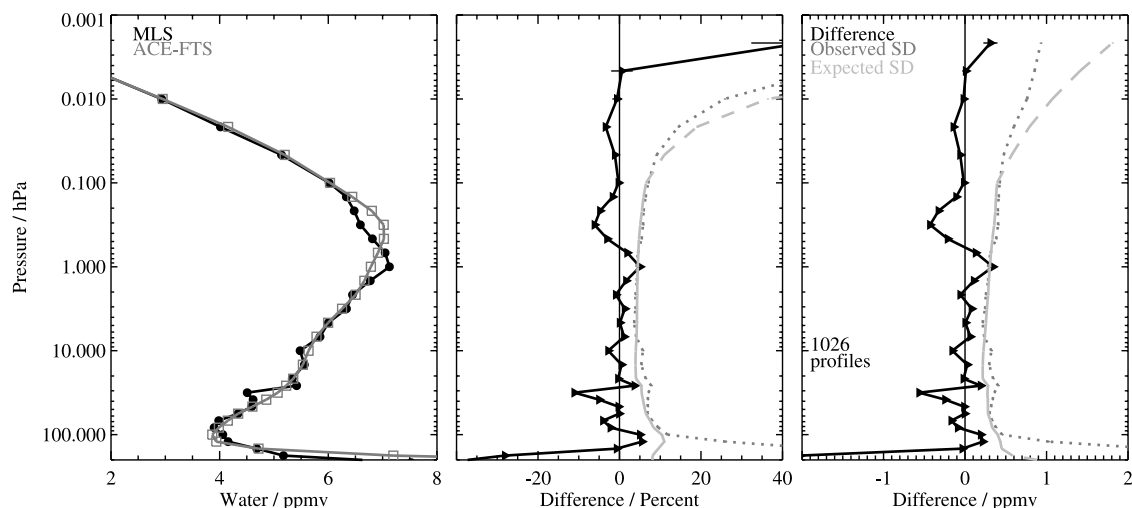
Figure 13. MLS H$_2$O compared to ACE-FTS averaged over 121 d of collocated data. (left) Global ensemble mean profiles of the collocated matches for both instruments (MLS, black circles; ACE-FTS, dark gray squares). (middle) Mean percentage difference profiles between the two measurements (MLS-ACE-FTS) (black triangles); standard deviation about the mean differences (Observed SD; dark gray dotted line) and the percentage root sum square of the precisions on both instrument measurements (Expected SD; light gray dashed line). (right) As in Figure 13 (middle) except plotted in mixing ratio units.

orbit in September 1991 and uses infrared solar occultation in four radiometer channels and four radiometer/gas-filter correlation channels in the spectral region 2.45–10.0 μm to measure atmospheric temperature, aerosols, and composition including H$_2$O in the 6.6 μm band. Nominally, fifteen sunrise and sunset profiles are obtained per day. The latitude coverage is 80°S–80°N; the vertical range is from 15–85 km with a vertical resolution of 2.3 km and typical precisions of ~1–15% in the stratosphere for H$_2$O. The version 19 (v19) HALOE data set is used; this has been described by *Harries et al.* [1996] and in the SPARC water vapor report [*Kley et al.*, 2000]. The HALOE data are prescreened for cloud effects before distribution.

[50] As discussed by *McHugh et al.* [2005], H$_2$O comparisons should be limited to pressures >0.02 hPa because

of the possible contamination of the HALOE H$_2$O data by polar mesospheric clouds (PMCs) at certain times of the year. Figure 16 compares all coincident profiles obtained within ±1° in latitude, ±8° in longitude, and ±12 h from 53 d of HALOE data. MLS H$_2$O is larger than HALOE by 2–10% in the pressure range 68–1.5 hPa (apart from the 31.6–26.1 hPa levels). For pressures ≤1 hPa the bias is in the range 10–15%. Very similar results were found when the analysis was repeated for the separate HALOE sunrise/sunset events (not shown). The HALOE H$_2$O data have been previously reported as having a 5% dry bias in the stratosphere [*Kley et al.*, 2000] and this is consistent with the results of this comparison. The observed and expected SD are in good agreement in the pressure range 68–2.2 hPa,
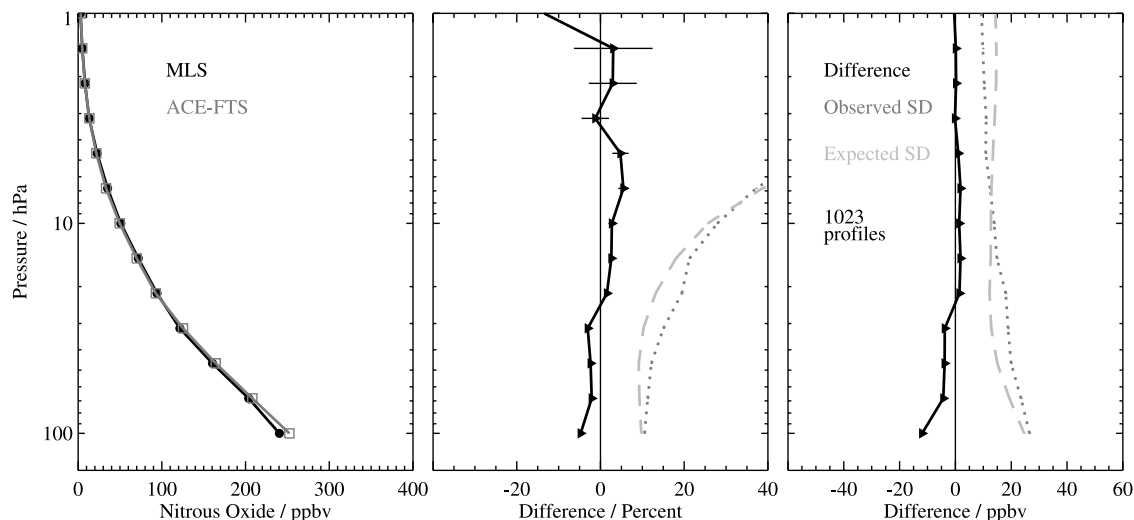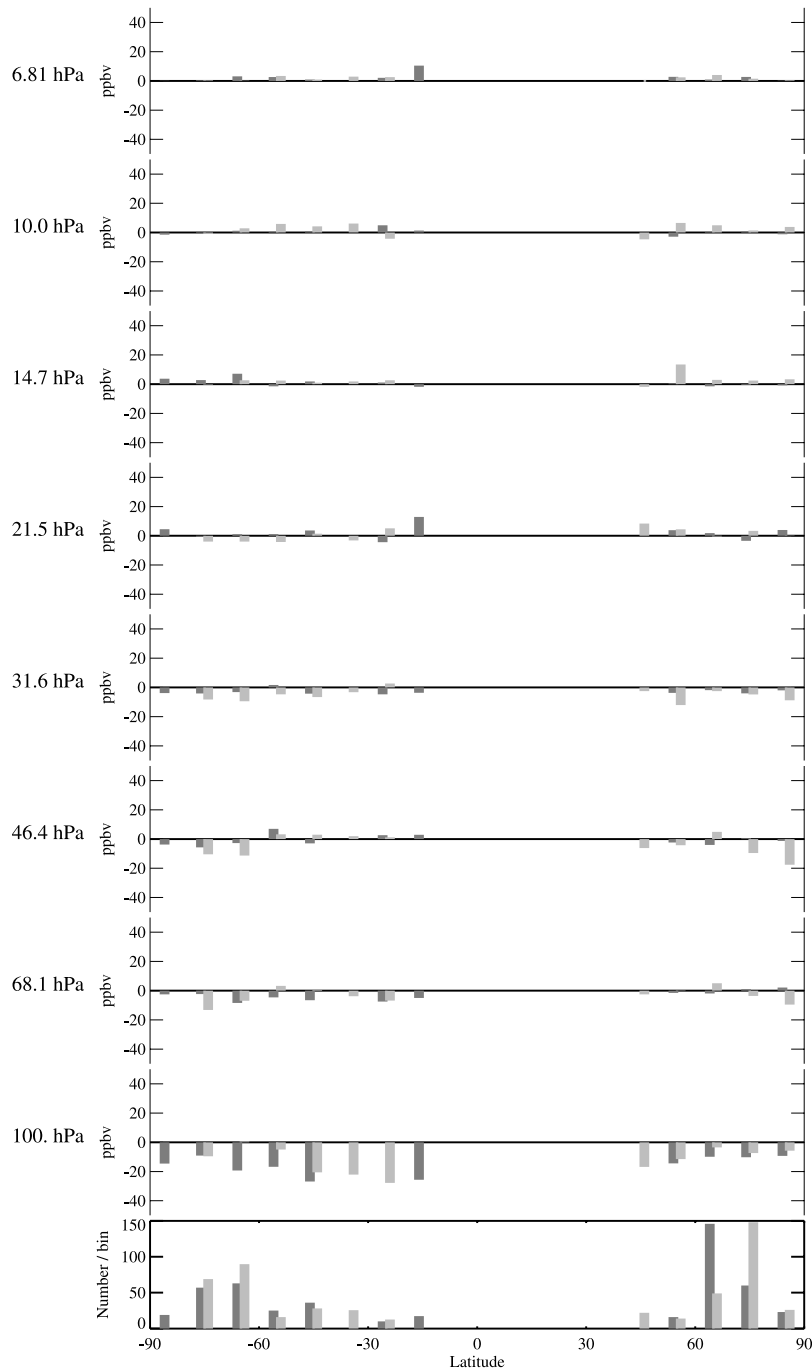

Figure 14. As Figure 13 except for ACE-FTS N$_2$O.

Figure 15. MLS N$_2$O compared to ACE-FTS for 121 d of collocated data. Distributions of the mean (MLS−ACE-FTS) N$_2$O mixing ratio differences in 10° latitude bins for sunrise (dark gray) and sunset (light gray) collocated profiles. Only latitude bins containing at least 10 collocated profiles are plotted. The bottom plot shows the number of sunrise/sunset occultations in each latitude bin.

where the HALOE precisions (not shown) are comparable to those from MLS.

3.1.3. SAGE II

[51] The Stratospheric Aerosol and Gas Experiment II (SAGE II) [*McCormick*, 1987] was launched into a 57° inclination orbit in October 1984 on the Earth Radiation Budget Satellite (ERBS). SAGE II uses ultraviolet/visible solar occultation in seven channels from 380 to 1020 nm to measure aerosol extinction at four wavelengths and the concentrations of O$_3$, H$_2$O and NO$_2$. The latitude coverage is 70°S−70°N and the vertical range is from cloud tops to 70 km with a resolution of ∼0.5 km. Fifteen sunrise and sunset profiles are obtained per day, although since November 2000 SAGE II has been operated with a 50% duty cycle. The version 6.2 [*Taha et al.*, 2004] H$_2$O data uses a modified spectral filter band pass with the selected filter position (centered at 945 nm) and width determined by an empirical minimization of the mean bias of SAGE II
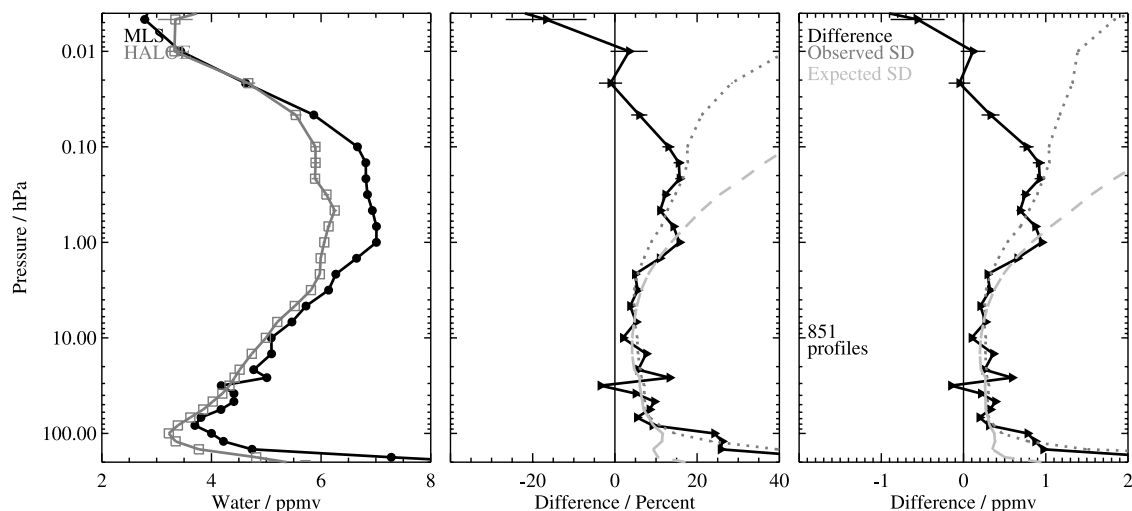
Figure 16. As Figure 13 except for HALOE H$_2$O averaged over 53 d of collocated data.

retrievals with respect to a 10-a (1992–2002) v19 HALOE climatology [*Thomason et al.*, 2004]. The agreement with HALOE is within 10% in the altitude range 15–40 km. Typical precisions for H$_2$O are ~15–35% in the stratosphere. The SAGE II H$_2$O data were screened as recommended to remove data points with correspondingly high aerosol extinctions (1020 nm extinction >2 × 10^{-4}).

[52] Figure 17 compares all coincident profiles obtained within ±1° in latitude, ±8° in longitude, and ±12 h from 87 d of SAGE II data. MLS H$_2$O is larger than SAGE II by 5–10% (apart from the 31.6–26.1 hPa levels) in the pressure range 68–4.6 hPa with the bias changing sign in the upper stratosphere above this range which is consistent with the validation results of *Taha et al.* [2004]. Similar results were found when the analysis was repeated for the separate SAGE II sunrise/sunset events (not shown). The observed SD is significantly smaller than the expected SD and is most likely due to a pessimistic estimate of the SAGE II precisions, which are reported by *Chiou et al.* [2004] to be overestimated by a factor of 2–3 in the lower stratosphere.

3.1.4. POAM III

[53] The Polar Ozone and Aerosol Measurement III (POAM III) [*Lucke et al.*, 1999] was launched in March 1998 on the French Space Agency SPOT-4 satellite into a polar Sun-synchronous orbit and uses ultraviolet/visible solar occultation in nine spectral channels in the region 345–1018 nm to measure aerosol extinction at six wavelengths and the concentrations of O$_3$, H$_2$O and NO$_2$. The H$_2$O observations use differential channels (on-peak/off-peak) in the 940 nm band. Fourteen sunrise and sunset profiles are obtained per day. However, to extend the instrument lifetime, the nominal observing scheme was changed to alternate between sunrise and sunset observations after the first year of operation, giving an effective 50% duty cycle. The latitude coverage is 63–88°S (all spacecraft sunset observations, but corresponding to local sunrise from mid-April to mid-September else local sunset) and 55–71°N (all spacecraft sunrise observations, but corresponding to local sunset) and the vertical range is from cloud tops to 50 km with a vertical resolution of 1–
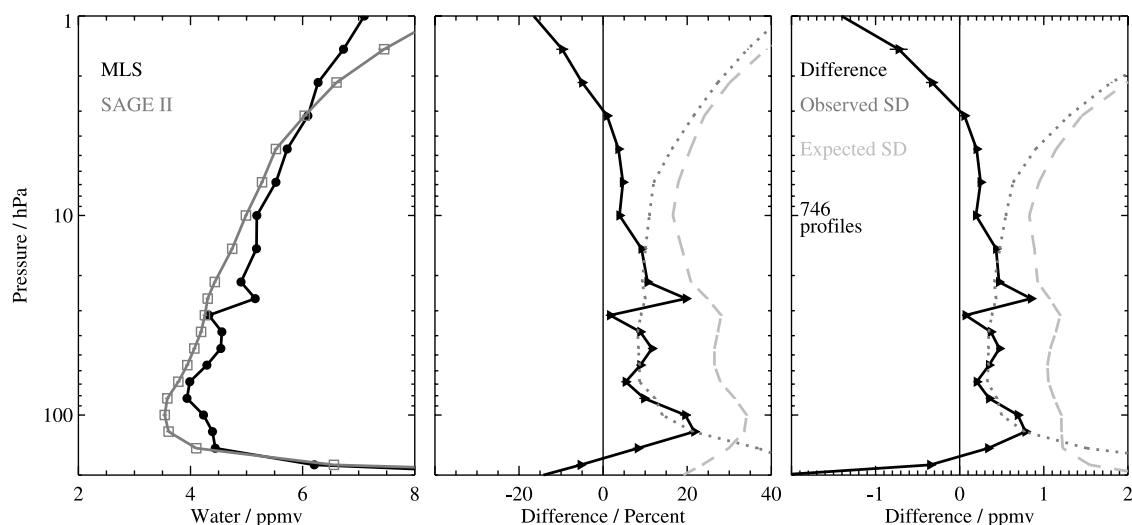

Figure 17. As Figure 13 except for SAGE II H$_2$O averaged over 87 d of collocated data.
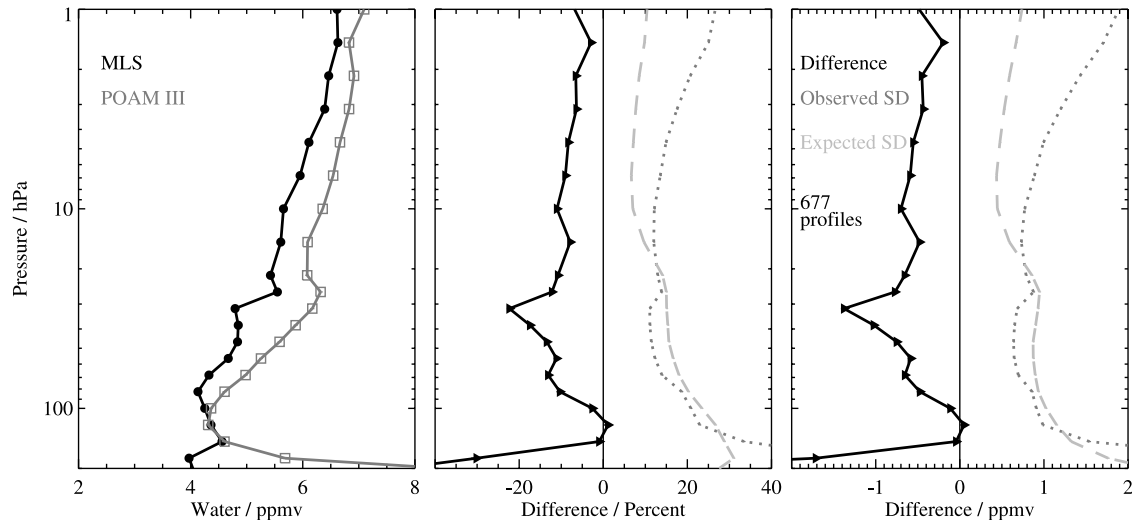
Figure 18. As Figure 13 except for POAM III H$_2$O averaged over 92 d of collocated data.

1.5 km which degrades to 3 km at 40 km. Typical precisions for H$_2$O are 5–7% in the stratosphere. The version 4 POAM III data set is used here [*Lumpe et al.*, 2006] and the H$_2$O data were screened for sunspot errors and aerosol contamination.

[54] Figure 18 compares all coincident profiles obtained within ±1° in latitude, ±8° in longitude, and ±12 h from 92 d of POAM III data. MLS H$_2$O is smaller than POAM III by 10% over most of the range 68–1 hPa (apart from the 31.6–26.1 hPa levels). In a repeat of the analysis for the separate POAM III spacecraft sunrise/sunset events (not shown), the sunset events were found to give a 5–10% larger negative bias (MLS–POAM III) than the sunrise. These results are consistent with the POAM III validation analysis of *Lumpe et al.* [2006] who report for the 12–35 km range a high bias of 5–10% for sunrise events and an additional ~10% greater bias for sunset. The observed and expected SD are in reasonable agreement for pressures >10 hPa.

3.1.5. MIPAS

[55] The Michelson Interferometer for Passive Atmospheric Sounding (MIPAS) [*Fischer and Oelhaf*, 1996] was launched on the European Space Agency (ESA) Environmental Satellite (Envisat) in March 2002 into a 98.5° inclination orbit. MIPAS is a Fourier Transform Spectrometer detecting the limb emission in the infrared spectral region 685–2410 cm^{-1} (4.15–14.6 μm) with a spectral resolution of 0.025 cm^{-1}. MIPAS operations were suspended in March 2004 because of an interferometer mechanism anomaly and then were restarted in January 2005 with a degraded spectral resolution of 0.0625 cm^{-1} and modified duty cycle and scan sequence to extend instrument lifetime [*Piccolo and Dudhia*, 2007]. MIPAS observes temperature, aerosols and a large number of minor constituents including H$_2$O and N$_2$O. The horizontal along-track sampling interval of the MIPAS measurements taken in the
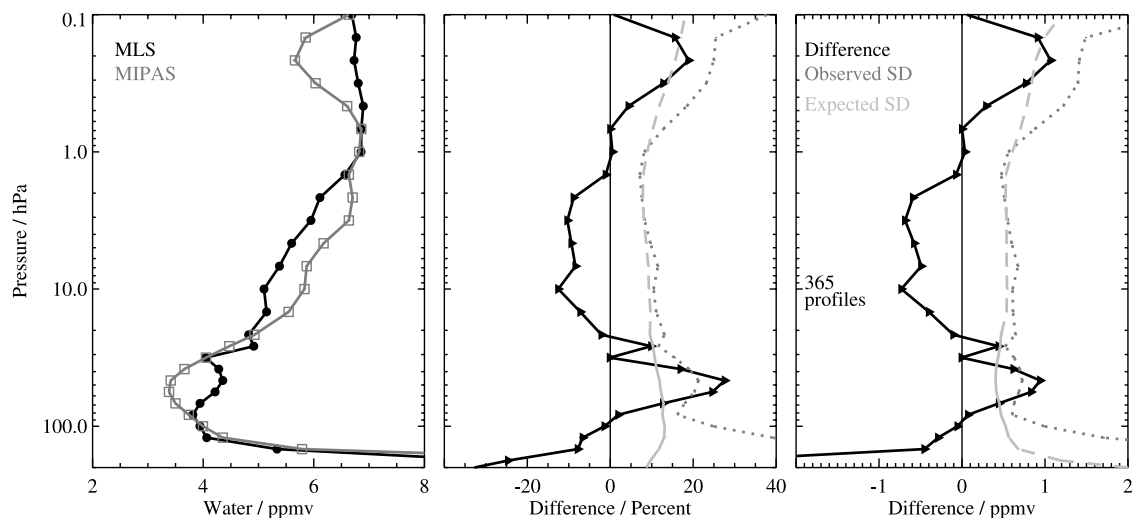

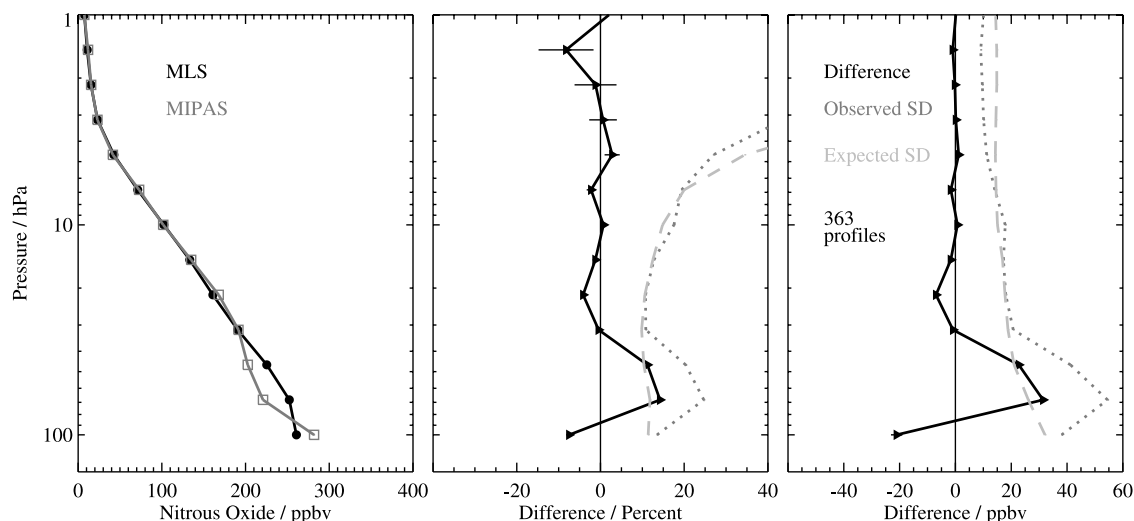**Figure 19.** As Figure 13 except for MIPAS H$_2$O on 28 January 2005.

Figure 20. As Figure 13 except for MIPAS N₂O on 28 January 2005.

nominal reduced resolution mode is ∼410 km, latitude coverage is 90°S–90°N, and the vertical sampling is ∼1.5–4 km with a vertical range 6–70 km. In addition to the ESA operational data products [*Raspollini et al.*, 2006], several institutions funded by the ENVISAT Calibration/Validation Program have developed off-line data processing capabilities for MIPAS. Here we show comparisons with off-line MIPAS H₂O and N₂O retrievals from algorithms developed at the University of Oxford (A. Dudhia and C. Waymark, personal communication, 2006). The MIPAS profiles were supplied with a cloud flag for data screening.

[56] Figures 19 and 20 and compare all coincident profiles obtained within ±1° in latitude, ±4° in longitude, and ±12 h for 28 January 2005.

3.1.5.1. H₂O

[57] MLS is smaller than MIPAS by ∼10% in the pressure range 22–2.2 hPa, and there are positive biases of ∼20% at 0.2 hPa and 25% at 46 hPa, but no significant bias in the pressure range 1.5–0.68 hPa. The observed and expected SD show good reasonable agreement in the pressure range 22–0.68 hPa.

3.1.5.2. N₂O

[58] MLS and MIPAS agree to about ±5% in the pressure range 32–1 hPa. The 68–46 hPa pressure region shows a positive bias of ∼10–15% and the 100 hPa level shows a negative bias of ∼10%. The observed and expected SD show good agreement in the pressure range 32–4.6 hPa.

3.1.6. Odin/SMR

[59] The Sub-Millimetre Radiometer (SMR) [*Murtagh et al.*, 2002] was launched on the Odin Satellite in February 2001 into a Sun-synchronous near polar 97.8° inclination orbit and uses submillimeter wave heterodyne spectroscopy to detect limb emission in the spectral region 486–581 GHz to measure atmospheric temperature and the concentrations of trace species including N₂O from retrievals at 502.296 GHz. The stratospheric measurement mode is time-shared with astronomy and other aeronomy modes and operates on one day out of three. The horizontal along-track sampling interval is ∼600 km, the latitude coverage is 82.5°S–82.5°N and the vertical scan range is 7–70 km. Profiles of N₂O are retrieved in the range ∼12–60 km with a

vertical resolution of 1.5 km in the lower stratosphere which degrades with increasing altitude to ∼3 km in the upper stratosphere [*Urban et al.*, 2005b, 2006]. The single-profile precision is in the range 10–30 ppbv. Operational Level 2 retrievals are produced by the Chalmers University of Technology (Göteborg, Sweden) and here we use the version 2.1 N₂O data which is similar to version 2.0 [*Urban et al.*, 2006]. The estimated systematic error is ≤12 ppbv above 20 km and in the range 12–35 ppbv below. An off-line reference processing system has been developed at the Observatoire Aquitain des Sciences de l'Univers (Floirac, France). The retrieval methodology and error characterization for the Chalmers version 1.2 data, and the differences between the French and Swedish data processing systems, are described in detail by *Urban et al.* [2005a]. *Barret et al.* [2006] compared the Bordeaux v222 reference version data to MLS 1.5 data, and *Urban et al.* [2006] describe the main differences between Chalmers v1.2, Bordeaux v222 and Chalmers v2.0 data and include a comparison with MIPAS off-line data. Only good quality SMR data points are included in these comparisons (i.e., assigned flag QUALITY = 0, and a measurement response for each retrieved mixing ratio larger than 0.75) to ensure that the information has been derived from the measurements, with negligible contribution from the a priori profile [*Urban et al.*, 2005b; *Barret et al.*, 2006].

[60] Figure 21 compares all coincident profiles obtained within ±1° in latitude, ±4° in longitude, and ±12 h from 60 d of SMR data. MLS N₂O is smaller than SMR by ≤5% in the pressure range 68–4.6 hPa and 10% smaller at 100 hPa. The observed and expected SD show reasonable agreement.

3.2. Ground-Based Instruments

[61] The Naval Research Laboratory (NRL) operates three Water Vapor Millimeter-wave Spectrometer (WVMS) [*Nedoluha et al.*, 1997] operates three instruments deployed at sites in the Network for the Detection of Atmospheric Composition Change (NDACC) which measure the emission from the 22 GHz H₂O transition. The data used here are daily averaged measurements from two NDACC sites: WVMS1 at the National Institute of Water and Atmospheres
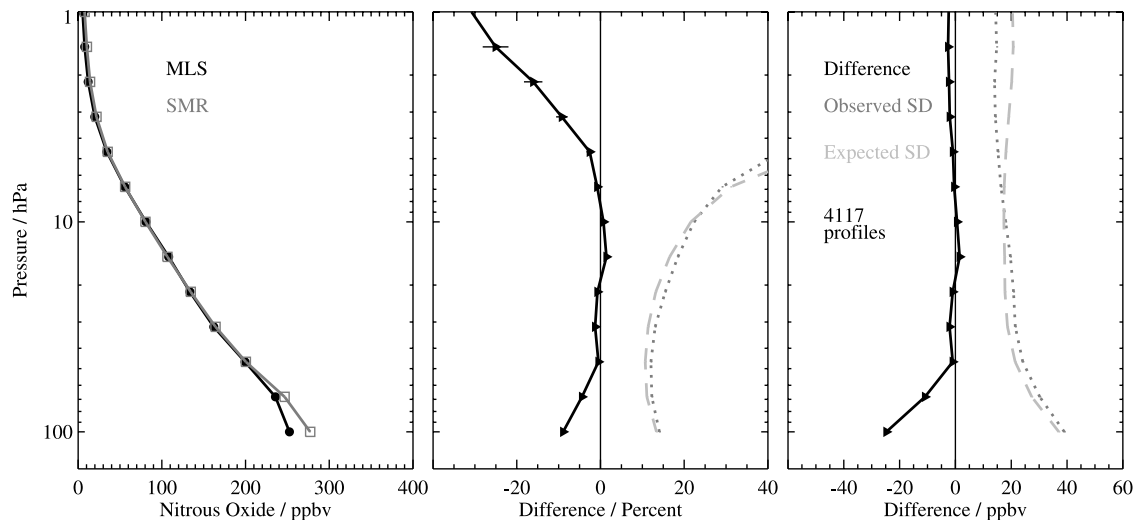
Figure 21. As Figure 13 except for SMR N$_2$O averaged over 60 d of collocated data.

Research (NIWA), Lauder, New Zealand (45.0°S, 169.7°E) and WVMS3 at the Mauna Loa Observatory, Hawaii (19.5°N, 204.4°E). The vertical range is 40–80 km with a vertical resolution of 10–20 km and typical precisions are 4–7% [*Neholuha et al.*, 1996]. In this case, since the MLS and WVMS instruments have quite different vertical resolutions, an appropriate intercomparison was achieved by first convolving the MLS retrievals with the WVMS averaging kernels [*Nedoluha et al.*, 2007] using methods described by *Rodgers and Connor* [2003]. The time sampling of the comparisons with the WVMS instruments is shown in Figure 12.

[62] Figures 22 and 23 compare all coincident profiles obtained within ±1° in latitude, ±8° in longitude, and ±12 h from 66 (58) d of Mauna Loa (Lauder) data. MLS H$_2$O and both WVMS sites agree to within ±5% for the pressure range 3.2–0.15 hPa, with a positive bias for pressures <0.32 hPa increasing to ~10% at 0.046 hPa. Time series comparisons of WVMS and v1.5 MLS H$_2$O by *Nedoluha et*

al. [2007] show good agreement in the seasonal and the interannual variations.

3.3. Balloon-Borne Instruments

[63] In this section we consider the data from in situ and remote sounding balloon-borne instruments obtained during two Aura validation campaigns at Fort Sumner, NM (34.4°N, 104.2°W), in September 2004 and September 2005.

3.3.1. Observations of the Middle Stratosphere (OMS) Gondola

[64] The in situ measurements presented are from two instruments flown on the OMS gondola that provided measurements of N$_2$O. The vertical range is typically from the upper troposphere to 32 km.

[65] The Lightweight Airborne Chromatograph Experiment (LACE) [*Moore et al.*, 2003] is a three-channel gas chromatograph which provides in situ profiles of various gases including N$_2$O. The precision is estimated to be 1–
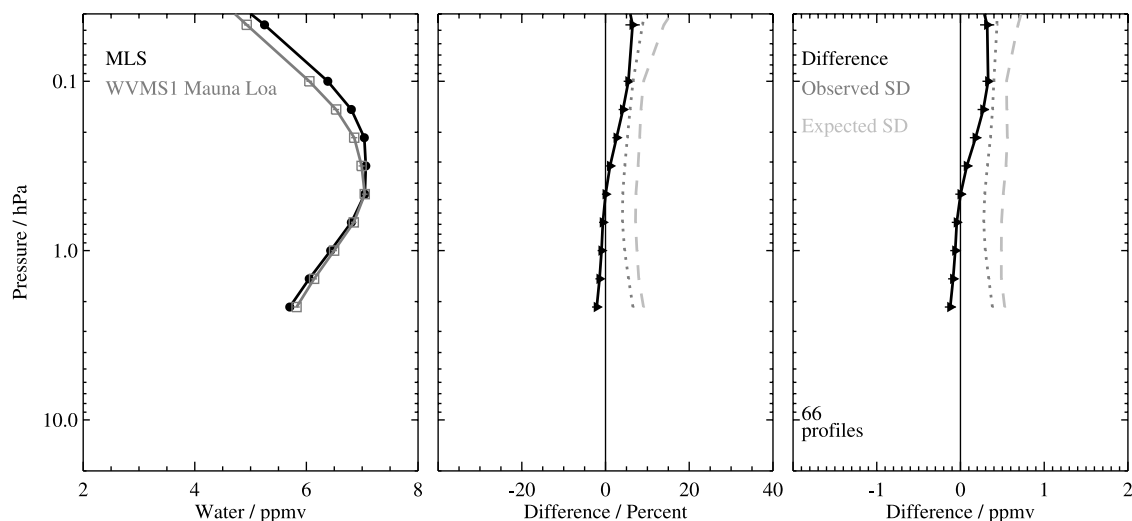

Figure 22. As Figure 13 except for WVMS Mauna Loa H$_2$O averaged over 66 d of collocated data. The MLS retrievals have been convolved with the WVMS Mauna Loa averaging kernels.
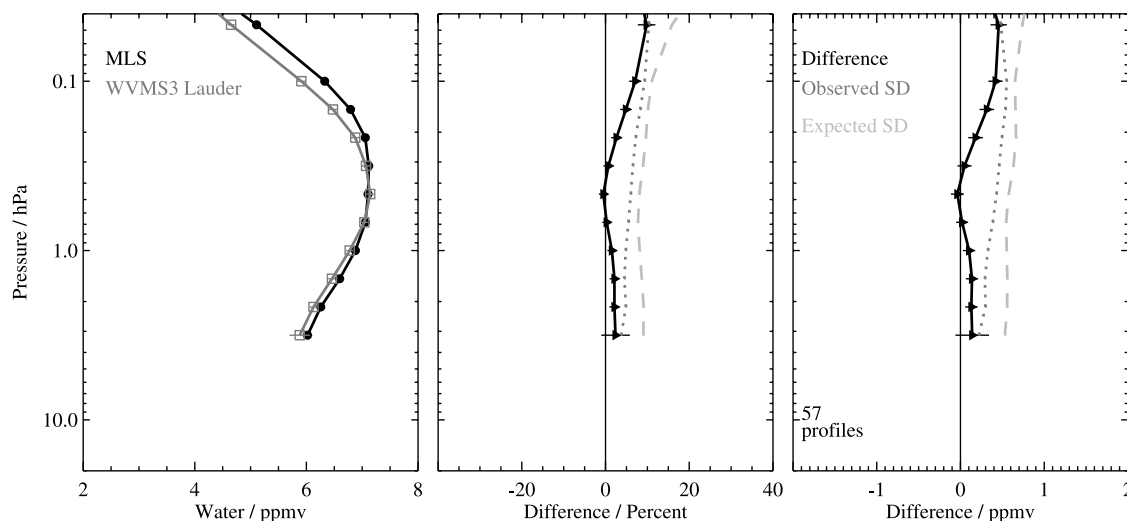
Figure 23. As Figure 13 except for WVMS Lauder H_2O averaged over 58 d of collocated data. The MLS retrievals have been convolved with the WVMS Lauder averaging kernels.

2% and the vertical resolution is 0.3 km. The Cryogenic Whole Air Sampler (CWAS) [*Hurst et al.*, 2002] collects in situ air samples in canisters which are analyzed for N_2O using electron-capture gas chromatography. The precision is estimated to be 1% and the vertical resolution is 0.3 km.

3.3.2. Balloon Observations of the Stratosphere (BOS) Gondola

[66] The remote sounding measurements presented are from three instruments flown on the BOS gondola that provided measurements of H_2O and N_2O.

[67] The Jet Propulsion Laboratory (JPL) MkIV instrument [*Toon*, 1991] is a Fourier Transform Infrared (FTIR) spectrometer operated in solar occultation mode that measures over the entire $650-5650$ cm^{-1} region with 0.01 cm^{-1} resolution. The vertical range is $8-40$ km with a vertical resolution of $2-3$ km. The MkIV H_2O retrievals use 13 spectral channels in the $1500-4630$ cm^{-1} and the N_2O retrievals use 46 spectral channels in the $1183-4725$ cm^{-1} region. The Smithsonian Astrophysical Observatory (SAO) [*Johnson et al.*, 1995] far-infrared spectrometer (FIRS)-2 is an FTIR spectrometer which measures the limb emission at midinfrared and far-infrared wavelengths between 6 and 120 μm with a 0.004 cm^{-1} resolution. The H_2O retrievals use 26 rotational transitions in both the far and mid infrared channels between 80 and 480 cm^{-1}. The transitions at higher frequency tend to add most of the weight to the retrievals in the upper troposphere and lower stratosphere, while the lower frequency transitions give more weight in the middle and upper stratosphere. The N_2O retrievals use 33 microwindows in the ν_2 rovibrational band between 549 and 590 cm^{-1}. The vertical range is $8-40$ km with a vertical resolution of $2-3$ km. The JPL Submillimeterwave Limb Sounder-2 (SLS-2), an updated version of the instrument described by *Stachnik et al.* [1999], is a cryogenic heterodyne spectroradiometer which measures the limb emission near 640 GHz with high resolution (2 MHz minimum channel width) for a number of species including N_2O. The vertical range is $15-45$ km with a vertical resolution of $2-3$ km below the balloon float altitude and $5-6$ km above.

3.3.3. Fort Sumner Comparisons

[68] The closest matching MLS profiles satisfy the coincidence criteria of $\pm1°$ in latitude, $\pm12°$ in longitude, and ±12 h with respect to the balloon measurement locations.

3.3.3.1. Comparison for 17 September 2004

[69] Figure 24 shows the N_2O comparison for the 17 September 2004 OMS flight (LACE). The MLS N_2O data show good agreement with respect to the 1-σ uncertainties and, except for the $46-32$ hPa pressure levels, which are biased slightly low, the overall shape of the LACE measurements is well represented.

3.3.3.2. Comparisons for 23–24 September 2004

[70] Figure 25 shows the H_2O and N_2O comparisons for the $23-24$ September 2004 BOS flight (JPL MkIV and FIRS-2). The MLS H_2O data show good agreement with both MkIV and FIRS-2 within the 1-σ uncertainties for pressures ≤46 hPa. At $68-56$ hPa MLS is biased low by ~0.3 ppmv and at $32-26$ hPa an oscillation is apparent. The MLS N_2O data show good agreement with the MkIV data within the 1-σ uncertainties and capture the overall shape of the MkIV measurements. There is generally good agreement with the slope of the FIRS-2 data, but FIRS-2 does not show the rise in N_2O at $32-10$ hPa that is clearly seen by both MLS and MkIV. The N_2O feature is consistent with a dip in H_2O at the same levels as seen by all three instruments.

3.3.3.3. Comparison for 29 September 2004

[71] Figure 26 shows the N_2O comparison for the 29 September 2004 OMS flight (CWAS). The MLS N_2O data show reasonable agreement with the CWAS measurements although this particular comparison is 890 km distant.

3.3.3.4. Comparisons for 20–21 September 2005

[72] Figure 27 shows the H_2O and N_2O comparisons for the $20-21$ September 2005 BOS flight (JPL MkIV, FIRS-2, SLS-2). The MLS H_2O data show good agreement with the MkIV measurements with an overall slight low bias of ~0.3 ppmv for pressures ≤68 hPa and there is a reasonable comparison with the shape of the FIRS-2 data which shows a slight high bias ~0.3 ppmv relative to MkIV. At $32-$
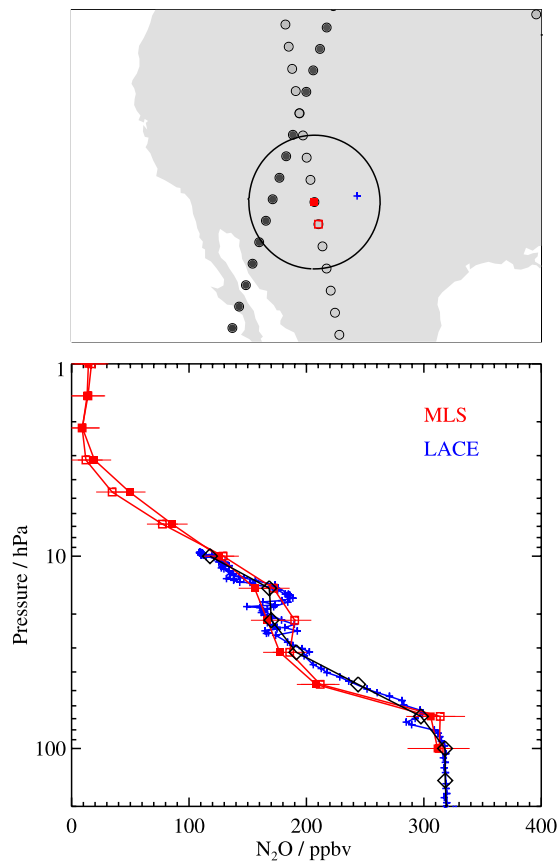
Figure 24. MLS N_2O ascending orbit overpass measurements (2029 UT) compared to the LACE measurements (1527–2014 UT) from the OMS gondola flown from Fort Sumner on 17 September 2004. The black diamond symbols joined by a solid line indicate the resulting convolution of the high-resolution LACE measurements (blue pluses) with the MLS averaging kernels. The location map shows the MLS overpass ascending (light circles) and descending orbit (dark circles) tangent points The two closest coincident MLS profiles (see text) are shown as solid (best match) and open red squares. The map scale is indicated by a 500 km radius locus centered on the best match. Horizontal error bars indicate the 1-sigma precisions. The correlative balloon instrument measurement locations are shown.

26 hPa an oscillation is apparent in the MLS data. The MLS N_2O data show good agreement with the MkIV data within the 1-σ uncertainties throughout the pressure range. There is also good agreement with FIRS-2 for pressures <68 hPa and these three instruments clearly show the rise in N_2O at 32–10 hPa. There is generally good overall agreement with the slope of the SLS-2 data, but SLS-2 does not show the N_2O feature seen by the other instruments. The N_2O feature is consistent with a dip in H_2O at the same levels as seen by MLS and MkIV.

4. Summary and Conclusions

[73] The quality and reliability of the Aura MLS H_2O and N_2O measurements have been presented for the version 2.2 (v2.2) data set which is expected to form the "definitive"

version of the MLS data for the next several years. Version 2.2 is the second public release of MLS data and has been used to process the incoming data stream since March 2007. Reprocessing of the data collected since MLS became operational in August 2004 is also in progress using the v2.2 algorithms. For this validation effort, 93 d of v2.2 data covering late 2004 to early 2007 were processed with an emphasis on special months or days of interest for validation (including campaigns). The impacts of the various
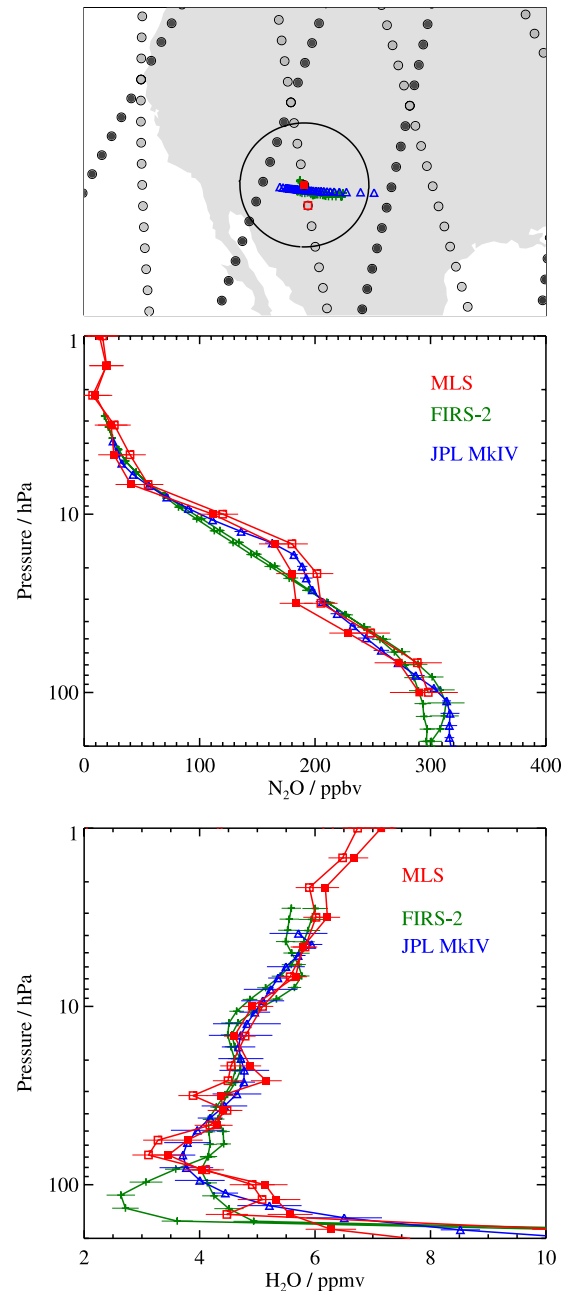

Figure 25. MLS N_2O and H_2O ascending orbit overpass measurements (23 September, 2035 UT) compared to the FIRS-2 (24 September, 0233 and 0454 UT) and JPL MkIV (24 September, 0000–0112 UT) measurements from the BOS gondola flown from Fort Sumner on 23–24 September 2004. Horizontal error bars indicate the 1-sigma precisions. Location map details are as in Figure 24.
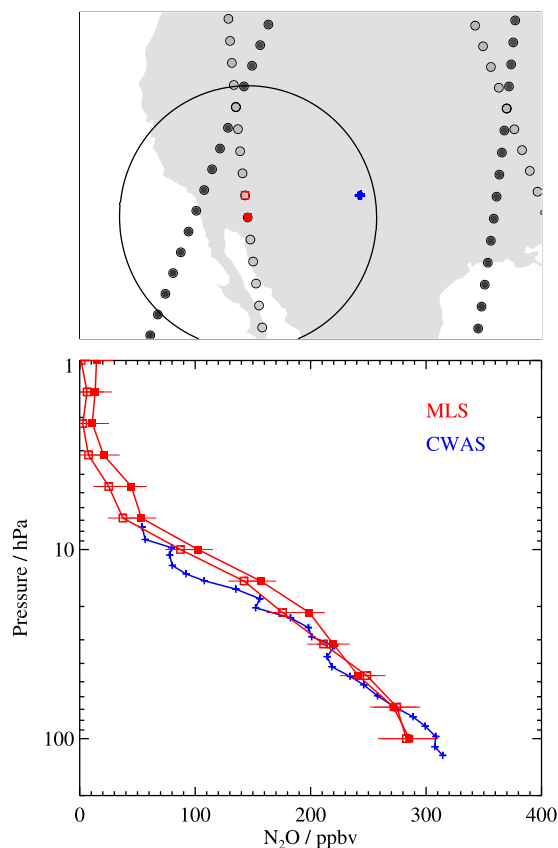
uncertainty analysis in section 2.6 is 0.2–0.5 ppmv (4–11%) in the pressure range 68–0.01 hPa. The scientifically useful range of the H$_2$O data is from 316 to 0.002 hPa. The results of statistical comparisons with correlative data sources show good agreement (apart from the 31.6–26.1 hPa
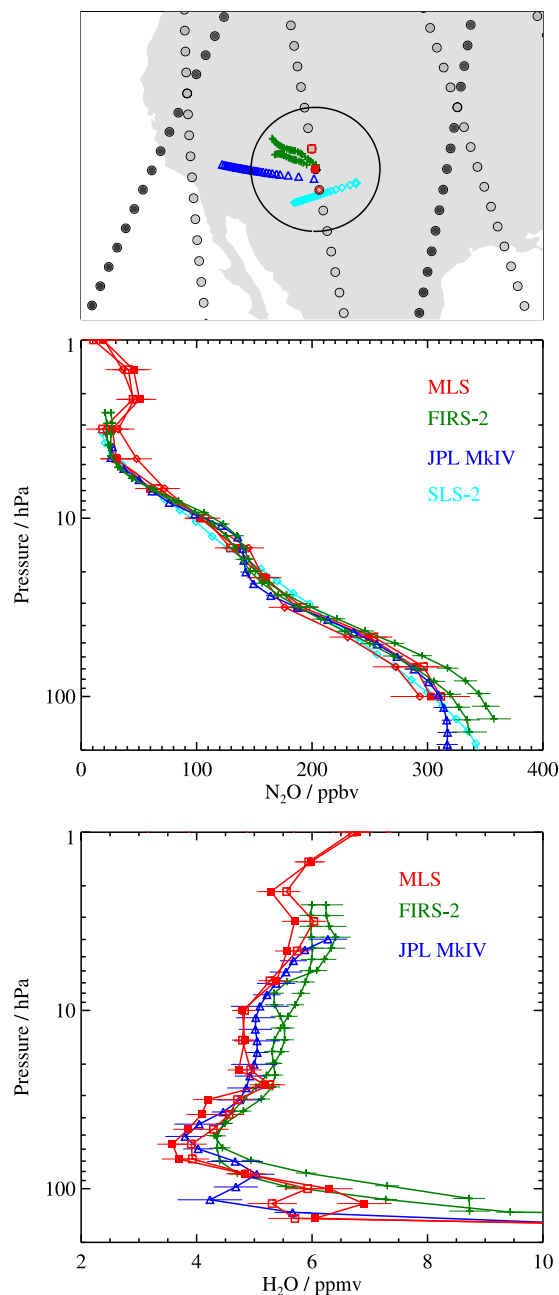

Figure 26. MLS N$_2$O ascending orbit overpass measurements (2054 UT) compared to the CWAS measurements (1637–2009 UT) from the OMS gondola flown from Fort Sumner on 29 September 2004. Horizontal error bars indicate the 1-sigma precisions. Location map details are as in Figure 24 except a 1000 km radius locus is centered on the closest matching MLS profile.

sources of systematic error have been estimated by a comprehensive set of retrieval simulations. Comparisons with correlative data sets from ground-based, balloon and satellite platforms operating in the UV/visible, infrared and microwave regions of the spectrum have been performed.

4.1. H$_2$O

[74] The stratospheric and mesospheric v2.2 H$_2$O data have been improved over v1.5 by providing higher vertical resolution in the lower stratosphere and better precision above the stratopause. However, a fine-scale oscillation in the v2.2 H$_2$O retrievals, possibly arising from the gain compression and pointing uncertainty effects described in section 2.6, causes the 31.6 hPa (26.1 hPa) level to be persistently low (high) by ∼0.4 ppmv (8%). Table 2 summarizes the main characteristics of the MLS v2.2 H$_2$O product.

[75] The single-profile precision is ∼0.2–0.3 ppmv (4–9%) and the vertical resolution is ∼3–4 km in the stratosphere. The precision and vertical resolution become worse with increasing height above the stratopause. Over the pressure range 0.1–0.01 hPa the precision degrades from 0.4–1.1 ppmv (6–34%) and the vertical resolution degrades to ∼12–16 km. The accuracy estimated from the systematic

Figure 27. MLS N$_2$O and H$_2$O ascending orbit overpass measurements (20 September, 2027 UT) compared to the FIRS-2 (20 September, 2034 and 2144 UT), JPL MkIV (21 September, 0043–0147 UT) and SLS-2 (20 September, 1750 UT) measurements from the BOS gondola flown from Fort Sumner on 20–21 September 2005. Horizontal error bars indicate the 1-sigma precisions. Location map details are as in Figure 24 except an additional MLS profile match (red diamond symbol) for N$_2$O is shown which matches better the SLS-2 measurement locations.

Table 2. Summary of the MLS v2.2 H_2O Product

Pressure,[a] hPa	Resolution: Vertical × Horizontal,[b] km	Precision[c]		Accuracy[d]		Comments
		ppmv	%	ppmv	%	
0.001	–	–	–	–	–	not recommended for scientific use
0.002	13 × 320	1.9	180	0.3	34	
0.004	13 × 360	1.5	82	0.3	16	
0.010	12 × 390	1.1	34	0.4	11	
0.022	12 × 420	0.8	18	0.4	9	
0.046	16 × 430	0.6	10	0.5	8	
0.10	14 × 440	0.4	6	0.5	8	
0.22	6.7 × 420	0.3	5	0.4	7	
0.46	5.5 × 410	0.3	4	0.5	6	
1.00	4.6 × 410	0.3	4	0.3	4	
2.15	4.0 × 380	0.2	4	0.3	5	
4.64	3.6 × 320	0.2	4	0.4	7	
10.0	3.3 × 280	0.2	4	0.5	9	
21.5	3.2 × 290	0.2	4	0.4	7	
46.4	3.1 × 240	0.3	6	0.2	4	
68.1	3.2 × 220	0.3	8	0.2	6	
≥82.3	–	–	–	–	–	see *Read et al.* [2007]

[a]Values in the table can be interpolated for intermediate pressure levels.
[b]Horizontal resolution in the along-track direction; across-track resolution is ∼7 km and the separation between adjacent retrieved profiles along the measurement track is 1.5° great circle angle (∼165 km).
[c]Precision on individual profiles; 1-σ estimate from the Level-2 algorithms.
[d]Systematic uncertainty; 2-σ estimate of the probable magnitude.

levels which show an additional ±8% bias): ACE-FTS ±5% for pressures 68–0.004 hPa; HALOE +2% to +10% for pressures 68–1.5 hPa; SAGE II +5% to +10% for pressures 68–4.6 hPa; POAM II -3% to −17% for pressures 68–1 hPa; MIPAS −10% to 0% for pressures 22–0.68 hPa; WVMS ±5% for pressures 3.2–0.15 hPa. The above values are consistent with the corresponding published biases for HALOE, SAGE II, POAM and WVMS. Individual collocated profile comparisons with the JPL MkIV and FIRS-2 balloon measurements show generally good agreement.

4.2. N_2O

[76] Substantial improvement has been achieved in the v2.2 N_2O data over v1.5 by reducing the significant low bias in the stratosphere that was reported by *Froidevaux et al.* [2006] and eliminating unrealistically high biased mixing ratios in the polar regions. Table 3 summarizes the main characteristics of the MLS v2.2 N_2O product.

[77] The single-profile precision is ∼13–16 ppbv (7–38%) and the vertical resolution is ∼4–5 km for the pressure range 46–4.6 hPa. The accuracy estimated from the systematic uncertainty analysis in section 2.6 is 3–32 ppbv (9–14%). The precision, resolution and accuracy become worse at higher pressures and for the 100–68 hPa levels the precision is ∼20–25 ppbv (8–9%), the vertical resolution is ∼5–6 km, and the estimated accuracy is 32–70 ppbv (13–25%). The scientifically useful range of the N_2O data is from 100 to 1 hPa. The results of statistical

Table 3. Summary of the MLS v2.2 N_2O Product

Pressure,[a] hPa	Resolution: Vertical × Horizontal,[b] km	Precision[c]		Accuracy[d]		Comments
		ppbv	%	ppbv	%	
≤0.68	–	–	–	–	–	not recommended for scientific use
1.00	6.5 × 300	14	250	0.6	12	
2.15	4.9 × 340	15	110	1.2	9	
4.64	4.1 × 370	14	38	3	9	
10.0	3.8 × 430	13	16	7	9	
21.5	4.1 × 490	13	9	19	13	
46.4	4.3 × 540	16	7	32	14	
68.1	5.6 × 590	20	8	32	13	
100	5.2 × 620	25	9	70	25	
147	–	–	–	–	–	not recommended for scientific use
≥215	–	–	–	–	–	not retrieved

[a]Values in the table can be interpolated for intermediate pressure levels.
[b]Horizontal resolution in the along-track direction; across-track resolution is ∼3 km and the separation between adjacent retrieved profiles along the measurement track is 1.5° great circle angle (∼165 km).
[c]Precision on individual profiles; 1-σ estimate from the Level-2 algorithms.
[d]Systematic uncertainty; 2-σ estimate of the probable magnitude.

comparisons with correlative data sources show good agreement: ACE-FTS ±5% for pressures 100–1 hPa; MIPAS ±5% for pressures 32–1 hPa; Odin/SMR 0% to −5% for pressures 68–4.6 hPa and −10% at 100 hPa. Individual collocated profile comparisons with the LACE, CWAS, JPL MkIV, JPL SLS-2 and FIRS-2 balloon measurements show generally good agreement.

4.3. Quality Control

[78] We have provided several quality control metrics in the MLS Level 2 files as discussed in section 2.2. To select data for scientific studies from the MLS v2.2 H$_2$O and N$_2$O products one should ensure that (1) the precision value for a data point is positive, (2) the "Status" field for the profile is even, (3) the "Quality" field for the profile is >0.9 for H$_2$O or >0.5 for N$_2$O, and (4) the "Convergence" field for the profile is <1.55 for N$_2$O. This test is not required for H$_2$O.

4.4. Future Improvements

[79] Validation of the Aura MLS measurements is an ongoing process that will continue as more v2.2 data become available and enable opportunities for cross comparisons with the recent January/February 2007 balloon flights from Kiruna, Sweden, active satellite missions and new deployments of instruments throughout the International Polar Year. Version 3 algorithms will address the problem of the oscillation in the H$_2$O retrievals at 32–26 hPa and the retrieval of N$_2$O may be extended to 147 hPa through the use of the 190-GHz measurements.

References

Barret, B., et al. (2006), Intercomparisons of trace gas profiles from the Odin/SMR and Aura/MLS limb sounders, *J. Geophys. Res.*, *111*, D21302, doi:10.1029/2006JD007305.

Bernath, P. F., et al. (2005), Atmospheric Chemistry Experiment (ACE): Mission overview, *Geophys. Res. Lett.*, *32*, L15S01, doi:10.1029/2005GL022386.

Boone, C. D., R. Nassar, K. A. Walker, Y. Rochon, S. D. McLeod, C. P. Rinsland, and P. F. Bernath (2005), Retrievals for the atmospheric chemistry experiment Fourier-transform spectrometer, *Appl. Opt.*, *44*, 7218–7231.

Chiou, E. W., L. W. Thomason, S. P. Burton, and H. A. Michelsen (2004), Assessment of the SAGE II version 6.2 water vapor data set through intercomparison with ATMOS/ATLAS-3 measurements, *Geophys. Res. Lett.*, *31*, L14101, doi:10.1029/2004GL020071.

Cofield, R. E., and P. C. Stek (2006), Design and field-of-view calibration of 114–660-GHz optics of the Earth Observing System Microwave Limb sounder, *IEEE Trans. Geosci. Remote Sens.*, *44*, 1166–1181.

Fischer, H., and H. Oelhaf (1996), Remote sensing of vertical profiles of atmospheric trace constituents with MIPAS limb-emission spectrometers, *Appl. Opt.*, *35*, 2787–2796.

Froidevaux, L., et al. (2006), Early validation analyses of atmospheric profiles from EOS MLS on the Aura satellite, *IEEE Trans. Geosci. Remote Sens.*, *44*, 1106–1121.

Harries, J. E., et al. (1996), Validation of measurements of water vapor from the Halogen Occultation Experiment (HALOE), *J. Geophys. Res.*, *101*, 10,205–10,216.

Hurst, D. F., et al. (2002), Construction of a unified, high-resolution nitrous oxide data set for ER-2 flights during SOLVE, *J. Geophys. Res.*, *107*(D20), 8271, doi:10.1029/2001JD000417.

Jarnot, R. F., V. S. Perun, and M. J. Schwartz (2006), Radiometric and spectral performance and calibration of the GHz bands of EOS MLS, *IEEE Trans. Geosci. Remote Sens.*, *44*, 1131–1143.

Jimenez, C. J., H. C. Pumphrey, I. A. MacKenzie, G. L. Manney, M. L. Santee, M. J. Schwartz, R. S. Harwood, and J. W. Waters (2006), EOS MLS observations of dehydration in the 2004–2005 polar winters, *Geophys. Res. Lett.*, *33*, L16806, doi:10.1029/2006GL025926.

Johnson, D. G., K. W. Jucks, W. A. Traub, and K. V. Chance (1995), Smithsonian stratospheric far-infrared spectrometer and data reduction system, *J. Geophys. Res.*, *100*, 3091–3106.

Kley, D., J. M. Russell III, and C. Phillips (2000), SPARC assessment of upper tropospheric and stratospheric water vapour, *WCCRP 113, WMO/TD-1043, SPARC Rep. 2*, World Clim. Res. Program, Geneva, Switzerland.

Livesey, N. J., and W. G. Read (2000), Direct retrieval of line-of-sight atmospheric structure from limb sounding observations, *Geophys. Res. Lett.*, *27*, 891–894.

Livesey, N. J., et al. (2005), Version 1.5 level 2 data quality and description document, Tech. Rep. JPL D-32381, Jet Propul. Lab., Pasadena, Calif.

Livesey, N. J., W. V. Snyder, W. G. Read, and P. A. Wagner (2006), Retrieval algorithms for the EOS Microwave Limb Sounder (MLS), *IEEE Trans. Geosci. Remote Sens.*, *44*, 1144–1155.

Livesey, N. J., et al. (2007), Version 2.2 level 2 data quality and description document, technical report, Jet Propul. Lab., Pasadena, Calif.

Lucke, R. L., et al. (1999), The Polar Ozone and Aerosol Measurement (POAM) III instrument and early validation results, *J. Geophys. Res.*, *104*, 18,785–18,799.

Lumpe, J., et al. (2006), Validation of Polar Ozone and Aerosol Measurement (POAM) III version 4 stratospheric water vapor, *J. Geophys. Res.*, *111*, D11301, doi:10.1029/2005JD006763.

Manney, G. L., N. J. Livesey, C. J. Jimenez, H. C. Pumphrey, M. L. Santee, I. A. MacKenzie, and J. W. Waters (2006), EOS microwave limb sounder observations of frozen-in anticyclone air in arctic summer, *Geophys. Res. Lett.*, *33*, L06810, doi:10.1029/2005GL025418.

Manney, G., et al. (2007), Solar occultation satellite data and derived meteorological products: Sampling issues and comparisons with Aura MLS, *J. Geophys. Res.*, doi:10.1029/2007JD008709, in press.

McCormick, M. P. (1987), SAGE II: An overview, *Adv. Space Res.*, *7*, 219–226.

McHugh, M., B. Magill, K. A. Walker, C. D. Boone, P. F. Bernath, and J. M. Russell (2005), Comparison of atmospheric retrievals from ACE and HALOE, *Geophys. Res. Lett.*, *32*, L15S10, doi:10.1029/2005GL022403.

Moore, F. L., et al. (2003), Balloonborne in situ gas chromatograph for measurements in the troposphere and stratosphere, *J. Geophys. Res.*, *108*(D5), 8330, doi:10.1029/2001JD000891.

Murtagh, D., et al. (2002), An overview of the Odin atmospheric mission, *Can. J. Phys.*, *80*, 309–319.

Neholuha, G. E., R. M. Bevilacqua, R. M. Gomez, W. B. Waltman, B. William, B. C. Hicks, D. L. Thacker, and W. A. Matthews (1996), Measurements of water vapor in the middle atmosphere and implications for mesospheric transport, *J. Geophys. Res.*, *101*, 21,183–21,193.

Nedoluha, G. E., et al. (1997), A comparative study of mesospheric water vapor measurements from the ground-based water vapor millimeter-wave spectrometer and space-based instruments, *J. Geophys. Res.*, *102*, 16,647–16,661.

Nedoluha, G. E., et al. (2007), A comparison of middle atmospheric water vapor as measured by WVMS, EOS-MLS, and HALOE, *J. Geophys. Res.*, doi:10.1029/2007JD008757, in press.

Piccolo, C., and A. Dudhia (2007), Precision validation of MIPAS-Envisat products, *Atmos. Chem. Phys. Disc.*, *7*, 911–929.

Pickett, H. M. (2006), Microwave Limb Sounder THz module on Aura, *IEEE Trans. Geosci. Remote Sens.*, *44*, 1122–1130.

Raspollini, P., et al. (2006), MIPAS level 2 operational analysis, *Atmos. Chem. Phys.*, 6, 5605–5630.

Read, W. G., Z. Shippony, M. J. Schwartz, N. J. Livesey, and W. V. Snyder (2006), The clear-sky unpolarized forward model for the EOS Aura Microwave Limb Sounder (MLS), *IEEE Trans. Geosci. Remote Sens.*, 44, 1367–1379.

Read, W. G., et al. (2007), Aura Microwave Limb Sounder upper tropospheric and lower stratospheric H_2O and RHi validation, *J. Geophys. Res.*, doi:10.1029/2007JD008752, in press.

Rodgers, C. D. (1976), Retrieval of atmospheric temperature and composition from remote measurements of thermal radiation, *Rev. Geophys.*, 14, 609–624.

Rodgers, C. D. (2000), *Inverse Methods for Atmospheric Sounding: Theory and Practice*, World Sci., Singapore.

Rodgers, C. D., and B. J. Connor (2003), Intercomparison of remote sounding instruments, *J. Geophys. Res.*, 108(D3), 4116, doi:10.1029/2002JD002299.

Russell, J. M., et al. (1993), The Halogen Occultation Experiment, *J. Geophys. Res.*, 98, 10,777–10,797.

Schoeberl, M. R., et al. (2006), Overview of the EOS Aura mission, *IEEE Trans. Geosci. Remote Sens.*, 44, 1066–1074.

Schwartz, M. J., W. G. Read, and W. V. Snyder (2006), EOS MLS forward model polarized radiative transfer for Zeeman-split oxygen lines, *IEEE Trans. Geosci. Remote Sens.*, 44, 1182–1191.

Stachnik, R. A., R. Salawitch, A. Engel, and U. Schmidt (1999), Measurements of chlorine partitioning in the winter Arctic stratosphere, *Geophys. Res. Lett.*, 26, 3093–3096.

Taha, G., L. W. Thomason, and S. P. Burton (2004), Comparison of Stratospheric Aerosol and Gas Experiment (SAGE) II version 6.2 water vapor with balloon-borne and space-based instruments, *J. Geophys. Res.*, 109, D18313, doi:10.1029/2004JD004859.

Thomason, L. W., S. P. Burton, N. Iyer, J. M. Zawodny, and J. Anderson (2004), A revised water vapor product for the Stratospheric Aerosol and Gas Experiment (SAGE) II version 6.2 data set, *J. Geophys. Res.*, 109, D06312, doi:10.1029/2003JD004465.

Toon, G. C. (1991), The JPL MkIV interferometer, *Opt. Photon News*, 2, 19–21.

Urban, J., et al. (2005a), Odin/SMR limb observations of stratospheric trace gases: Level 2 processing of ClO, N_2O, HNO_3, and O_3, *J. Geophys. Res.*, 110, D14307, doi:10.1029/2004JD005741.

Urban, J., et al. (2005b), Odin/SMR limb observations of stratospheric trace gases: Validation of N_2O, *J. Geophys. Res.*, 110, D09301, doi:10.1029/2004JD005394.

Urban, J., et al. (2006), Odin/SMR limb observations of trace gases in the polar lower stratosphere during 2004–2005, in *Proceedings of the ESA First Atmospheric Science Conference, 8–12 May 2006, Frascati, Italy*, edited by H. Lacoste, *Eur. Space Agency Spec. Publ., ESA-SP-628*.

Waters, J. W. (1993), Microwave limb sounding, in *Atmospheric Remote Sensing by Microwave Radiometry*, edited by M. A. Janssen, chap. 8, pp. 383–496, John Wiley, New York.

Waters, J. W., et al. (2006), The Earth Observing System Microwave Limb Sounder (EOS MLS) on the Aura satellite, *IEEE Trans. Geosci. Remote Sens.*, 44, 1075–1092.

World Meteorological Organization (2006), Scientific assessment of ozone depletion, *Global Ozone Res. and Monit. Proj. Rep.*, 50, Geneva, Switzerland.

Wu, D. L., et al. (2007), Validation of the Aura MLS cloud ice water content (IWC) measurements, *J. Geophys. Res.*, doi:10.1029/2007JD008931, in press.

————————

E. Atlas, Division of Marine and Atmospheric Chemistry, University of Miami, Coral Gables, FL 33149, USA.

P. F. Bernath, Department of Chemistry, University of York, York YO10 5DD, UK.

C. D. Boone, Department of Chemistry, University of Waterloo, 200 University Avenue W., Waterloo, ON, Canada N2L 3G1.

R. E. Cofield, D. T. Cuddy, W. H. Daffer, B. J. Drouin, L. Froidevaux, R. A. Fuller, R. F. Jarnot, B. W. Knosp, A. Lambert (corresponding author), N. J. Livesey, V. S. Perun, H. M. Pickett, W. G. Read, M. L. Santee, M. J. Schwartz, W. V. Snyder, R. A. Stachnik, P. C. Stek, R. P. Thurstans, G. C. Toon, P. A. Wagner, J. W. Waters, and D. L. Wu, Jet Propulsion Laboratory, 4800 Oak Grove Drive, Pasadena, CA 91109, USA. (alyn.lambert@jpl.nasa.gov)

J. W. Elkins, Global Monitoring Division, Earth System Research Laboratory, NOAA, Boulder, CO 80305, USA.

C. Jimenez and H. C. Pumphrey, School of GeoSciences, University of Edinburgh, Edinburgh EH9 3JW, UK.

K. W. Jucks, Harvard-Smithsonian Center for Astrophysics, Cambridge, MA 02138, USA.

G. L. Manney, Department of Physics, New Mexico Institute of Mining and Technology, Socorro, NM 87801, USA.

D. Murtagh and J. Urban, Department of Radio and Space Science, Chalmers University of Technology, SE-41296 Göteborg, Sweden.

G. E. Nedoluha, Remote Sensing Division, Naval Research Laboratory, Washington, DC 20375-5000, USA.

K. A. Walker, Department of Physics, University of Toronto, Toronto, ON, Canada M5S 1A7.